**Regulatory T cells promote myelin regeneration in the Central Nervous System**

Yvonne Dombrowski[1], Thomas O'Hagan[1], Marie Dittmer[1], Rosana Penalva[1], Sonia R. Mayoral[4], Peter Bankhead[2], Samara Fleville[1], George Eleftheriadis[1], Chao Zhao[3], Michelle Naughton[1] Rachel Hassan[1], Jill Moffat[1], John Falconer[1], Amanda Boyd[8], Peter Hamilton[2], Ingrid V. Allen[1], Adrien Kissenpfennig[1], Paul N. Moynagh[1,5], Emma Evergren[2], Bernard Perbal[6,7], Anna C. Williams[8], Rebecca J. Ingram[1], Jonah R. Chan[4], Robin J.M. Franklin[3] and Denise C. Fitzgerald[1,*]

[1]Centre for Experimental Medicine, School of Medicine, Dentistry and Biomedical Science, Queen's University Belfast, Northern Ireland, UK

[2]Centre for Cancer Research and Cell Biology, School of Medicine, Dentistry and Biomedical Science, Queen's University Belfast, Northern Ireland, UK

[3]Wellcome Trust-Medical Research Council Cambridge Stem Cell Institute, Clifford Allbutt Building, Cambridge Biomedical Campus, University of Cambridge, UK

[4]Department of Neurology and Program in Neurosciences, University of California, San Francisco, USA

[5]Institute of Immunology, Department of Biology, National University of Ireland Maynooth, Ireland.

[6]Université Paris 7- D. Diderot, Paris, France

[7]Université Côte d'Azur, CNRS, GREDEG, France and International CCN Society

[8]Centre for Regenerative Medicine, University of Edinburgh, Edinburgh, UK

*Correspondence: d.fitzgerald@qub.ac.uk

**Summary**

**Regeneration of central nervous system (CNS) myelin involves differentiation of oligodendrocytes from oligodendrocyte progenitor cells (OPC). In multiple sclerosis (MS), remyelination can fail despite abundant OPC in lesions, suggesting impairment of oligodendrocyte differentiation. Various T cells are present in the CNS of MS patients yet the role of T cells in remyelination has received little attention. Here we report a new function of regulatory T cells (Treg) in promoting oligodendrocyte differentiation and (re)myelination. Treg-deficient mice exhibited significantly impaired remyelination and fewer differentiated oligodendrocytes that was rescued by adoptive transfer of Treg *in vivo*. In brain slice cultures, Treg accelerated developmental myelination and remyelination, even in the absence of overt inflammation. Treg directly promoted OPC differentiation *in vitro* and myelination in OPC-dorsal root ganglion neuron co-cultures. We identified CCN3 as a novel Treg-derived protein that was both necessary and sufficient for Treg-induced oligodendrocyte differentiation and brain slice myelination *in vitro*. This is the first evidence of CCN3 in CNS regeneration and of CCN3 production by T cells. These findings point to a new regenerative function of Treg in the CNS, distinct from immunomodulation. Although originally named 'Treg' to reflect immunoregulatory roles, this name also aptly captures emerging regenerative functions of Treg.**

The failure to reinvest demyelinated axons with new myelin sheaths results in a lack of axonal conduction and metabolic support. This ultimately leads to irreversible axonal loss that typifies later stages of chronic demyelinating diseases such as MS, leaving patients with permanent neurological disability[1,2]. Remyelination frequently occurs in the context of innate and adaptive immune responses[3,4]. T cells can act as effectors of myelin damage but are also required for successful remyelination[5]. However, T cells encompass a range of phenotypically and functionally distinct subsets and contributions of T cell subsets to CNS remyelination are poorly understood.

Since inflammation-resolving effects of Treg frequently coincide with tissue regeneration, we hypothesized that Treg promote remyelination.

To study regenerative T cell functions in remyelination *in vivo*, distinct from classical T cell-mediated demyelination observed in experimental autoimmune encephalomyelitis (EAE), focal demyelination was induced by injecting lysolecithin into spinal cord white matter of mice. Such lesions naturally remyelinate within one month and follow a well-defined time-course with distinct phases of OPC activation, recruitment and oligodendrocyte differentiation[6,7]. Flow cytometric immunophenotyping at 3 days post lesion (d.p.l.) demonstrated an abundance of $CD45^+CD11b^+$ myeloid cells in lesioned tissue as previously described[8]. However, distinct, albeit smaller populations of $CD3^+$ and $CD4^+$ T cells were also evident even up to 11 d.p.l., including $CD3^+CD4^+Foxp3^+$ Treg, a T cell population recently implicated in tissue regeneration[9,10] (Supplementary Fig. 1a-e). To determine if Treg were functionally important in remyelination, we used Foxp3-DTR transgenic mice in which diphtheria toxin (DT) administration depletes Foxp3-expressing cells[11] (Supplementary Fig. 1f). Chronic DT exposure causes toxicity and considerable morbidity even in wild-type mice[12-14] while Treg deficiency induces systemic immune activation[11], precluding long-term studies. Therefore, densities of $CC1^+Olig2^+$ differentiated oligodendrocytes, as an established surrogate readout of remyelination[15], were compared at 14 d.p.l. and electron microscopy was performed at 17 d.p.l.

Treg-depleted animals exhibited significantly fewer differentiated $CC1^+Olig2^+$ oligodendrocytes than non-depleted animals or DT-treated wild-type controls (Fig. 1a,b). Mice lacking Treg exhibited comparable lesion sizes (Fig. 1c) indicating that Treg are not required to limit tissue damage in this model and crucially, that experimental groups had comparable burdens of demyelination to repair. Reduced numbers of $CC1^+Olig2^+$ cells in Treg-depleted mice could have arisen because of a failure to recruit sufficient OPC to the demyelinated area. However, no significant differences in $Olig2^+Ki67^+$ proliferating OPC at 5 d.p.l. or 10 d.p.l. were observed between

groups (Fig. 1d and Supplementary Fig. 1g) indicating that reduced generation of oligodendrocytes was likely due to impairment in differentiation. Restricting Treg depletion only to the pre-lesioning phase did not alter $CC1^+Olig2^+$ cell numbers (Supplementary Fig. 1h), suggesting that Treg are important in later stages of remyelination. Indeed electron microscopic analysis of lesions demonstrated significantly fewer remyelinated axons in Treg-depleted animals (Fig. 1e). To further test the role of Treg in remyelination using a gain-of-function model, MACS-purified wild-type Treg were injected into Treg-deficient animals ('injected Treg'). Treg administration significantly increased numbers of $CC1^+Olig2^+$ differentiated oligodendrocytes in lesions, demonstrating the capacity of Treg to rescue impaired oligodendrocyte differentiation *in vivo* (Fig. 1f,g). To verify the importance of Treg in myelin regeneration in a second remyelinating model as well as at a different CNS site, demyelination was induced using cuprizone. Similar to results obtained using the spinal cord lysolecithin model, Treg depletion significantly impaired $CC1^+Olig2^+$ oligodendrocyte differentiation in the corpus callosum of cuprizone-treated mice at day 14 of the remyelination phase (Fig. 1h,i) but not at day 10 (Supplementary 1i). This finding was supported by reduced PLP mRNA expression in Treg-depleted animals at day 14 (Supplementary Fig. 1j). Treg depletion did not significantly affect overall oligodendrocyte lineage numbers (Supplementary Fig. 1k) emphasizing the predominant effect of Treg depletion on the differentiation phase of the regenerative response. These studies identify a novel role for Treg in the process of oligodendrocyte differentiation and CNS remyelination in both brain and spinal cord *in vivo*.

Next, we asked if Treg exerted direct regenerative effects within CNS tissue distinct from immunomodulation of infiltrating immune cells. To this end, we used neonatal murine organotypic brain slice cultures which naturally generate compact myelin *ex vivo* via OPC proliferation, differentiation and axonal ensheathment[16-19]. To determine if Treg influence myelination, FACS-purified $CD4^+Foxp3\text{-}eGFP^+$ natural Treg or control $CD4^+Foxp3^-$ conventional T cells (Tconv) were added directly onto slices. T cells infiltrated tissues and $GFP^+$ Treg were still detectable within slices

after 3 days *in vitro* (d.i.v.) (Supplementary Fig. 2a). Slices co-cultured with Treg cells contained significantly more $MBP^+$ oligodendrocytes and had significantly higher myelination index (myelin and axonal overlap, representing axonal ensheathment by myelin) at 3 d.i.v. than control slices without cells (Supplementary Fig. 2b-d) or slices with Tconv cells (Supplementary Fig. 2e). These findings demonstrate a myelinating action induced specifically by Treg, rather than by activated T cells in general.

To investigate mechanisms of Treg-induced myelination beyond cell-cell contact, slices were supplemented with conditioned media from $CD4^+$ T cells that were either polarized to a Treg phenotype or were non-polarized (NP) to serve as activated T cell controls (Supplementary Fig. 2f), or control medium. Treg-conditioned media significantly increased $MBP^+$ mature oligodendrocytes and myelination compared to controls (Fig. 2a-c, Supplementary Fig. 2g). These findings indicated that secreted factors drive oligodendrocyte differentiation and pro-myelinating effects of Treg.

To test if Treg also promoted regeneration of myelin, slices myelinated in culture for 14 days and were then demyelinated with lysolecithin. Addition of Treg-conditioned media for 7 days following demyelination significantly increased $MBP^+$ mature oligodendrocytes (Fig. 2d,f) and myelination index (Fig. 2e,f Supplementary movies) compared to controls. These increases represented an acceleration of remyelination by Treg as control slices eventually remyelinated after 2 weeks (data not shown). This was confirmed by electron microscopy showing significantly increased numbers of remyelinated axons in Treg-treated slices compared to control, remyelinating slices (Supplementary Fig. 2h-j).

Although brain slices lack peripheral immune cells, CNS-resident microglia and astrocytes can generate local inflammatory responses upon slicing and demyelination[20,21] and therefore, effects of Treg on (re)myelination could be due to known anti-inflammatory functions. Thus, to categorically test if Treg directly promoted CNS myelination rather than indirectly via immunoregulation, slices were equilibrated for one week after slicing[20] to allow pro-inflammatory cytokine production to subside (Supplementary Fig. 2k) prior to addition of T cell-conditioned media. In this model, slices

treated with Treg-conditioned media again exhibited significantly higher $MBP^+$ oligodendrocyte numbers (Fig. 2g,i) and myelination index (Fig. 2h,i) than controls. These findings show that Treg directly promote oligodendrocyte differentiation and myelin production under minimal-inflammatory conditions, suggesting a primary regenerative function of Treg in the CNS distinct from, but complementary to, known immunomodulatory functions.

To further investigate mechanisms of Treg-induced remyelination via OPC differentiation we next determined whether Treg directly influenced glial cells using mixed glial cultures containing OPC as well as astrocytes and microglia (Supplementary Fig. 3a). Treg-conditioned media significantly increased oligodendrocyte differentiation compared to control medium (Fig. 3a,b,d) and control non-polarized T cell-conditioned medium (Supplementary Fig. 3b,c), demonstrating direct Treg signaling to glia. This effect was consistent independent of whether Tregs were induced from total $CD4^+$ T cells or from naïve $CD4^+$ T cells (Supplementary Fig. 3d). Supporting our *in vivo* findings, we observed no difference in oligodendrocyte lineage cell numbers (Fig. 3c), proliferation (Fig. 3e,f) or survival (Supplementary Fig. 3e,f).

As proof of principle that Treg can directly modulate a regenerative cell population, independent of other CNS cells, pure OPC were cultured in the presence or absence of T cell-conditioned media. Within just two days, OPC treated with Treg-conditioned media exhibited significantly more $MBP^+$ differentiated oligodendrocytes (Fig. 3g,h) demonstrating a direct action of Treg on OPC. To test if this was functionally relevant, Treg-conditioned media were added to OPC-dorsal root ganglion (DRG) neuron co-cultures. Treg accelerated myelination of DRG neurons, evident within 4 days of stimulation with Treg-conditioned media (Fig. 3i,j). Although not ruling out additional indirect mechanisms, these findings show that Treg-secreted factors can directly signal to OPC to promote oligodendrocyte differentiation and functional myelination. This demonstrates for the first time that Treg can alter the regenerative capacity of CNS progenitor cells.

We next investigated Treg-secreted factors that enhanced oligodendrocyte differentiation and myelination. Analysis of conditioned media by proteome profiling identified a number of candidate factors relevant to regeneration (Supplementary Fig. 4a) including CCN3 a growth regulatory protein with bioactivity in extracellular, cytoplasmic and nuclear compartments and implicated in regeneration of various tissues[22-25]. Dual ELISA and western blot validation confirmed that CCN3 was produced by Treg (Fig. 4a,b). To determine if CCN3 mediated the oligodendrocyte-differentiating effect of Treg, CCN3 antibody was added to glial and brain slice cultures treated with Treg-conditioned media. Anti-CCN3 antibody abolished Treg-induced oligodendrocyte differentiation in glial cultures (Fig. 4c,d, Supplementary Fig. 4b) and inhibited the pro-myelinating effect of Treg in brain slice cultures (Fig. 4e). To confirm these findings with a second loss-of-function approach, CCN3 was depleted from Treg-conditioned media (Supplementary Fig. 4c, d) and recovered as eluted protein. Treg-conditioned media depleted of CCN3 failed to promote oligodendrocyte differentiation in glial cultures (Fig. 4f) or brain slice myelination (Fig. 4g,h). Furthermore, treatment with recovered CCN3 significantly enhanced brain slice myelination (Fig. 4g,h). These studies implicate CCN3 as a novel Treg-derived protein that mediates Treg-driven OPC differentiation and CNS myelination.

Immune-mediated tissue regeneration is an expanding field and recent studies highlight the importance of innate immune signaling in myelin regeneration[3,4,26]. Yet, despite decades of research into T cell-mediated pathogenesis and immunomodulation of CNS demyelination, very little is known about T cell functions in remyelination. Given that T cell-targeting therapies are used in MS, it is crucial to understand the full range of roles played by T cells. However, when interrogating immunoregenerative functions, appropriate choice of experimental models is crucial. Treg limit damage in many inflammatory disease models including EAE. Overlapping tissue damage and regeneration often occur in immune-mediated disease models such as EAE. Thus, true enhancement of regeneration can be challenging to distinguish from modulation of immunopathogenicity in these models. This motivated our choice of lysolecithin-induced demyelination in which the demyelinating

insult is time-limited, clearly defined anatomically, independent of immune-driven tissue damage and follows a well-defined course of highly efficient myelin regeneration. With this approach, in combination with other models without peripheral immune influence such as OPC and brain slice cultures, we have uncovered a key regenerative function of Treg. Mechanisms underlying this function include acceleration of oligodendrocyte differentiation and (re)myelination, via CCN3, a protein not previously known to target OPC, or indeed, to be produced by Treg.

CCN3 is a growth regulatory protein with bioactivity in extracellular, cytoplasmic and nuclear compartments and implicated in regeneration of various tissues[23-25,27,28]. CCN3 is expressed in the developing CNS[22,29] and glioma[30], but has not previously been implicated in CNS regeneration. Of note, we detected CCN3 expression in early organotypic brain slice cultures (data not shown) which may be developmentally regulated or due to tissue injury. In immune development, $CD34^+$ bone marrow progenitor cells express CCN3; however, ours is the first report that Treg, or indeed any T cell population, produces CCN3. Together, these findings identify CCN3 as an immune effector molecule from early innate immune development to resolution of adaptive immune responses. This potentially places CCN3 at the leading edge of immune-mediated tissue regeneration and warrants investigation in immune cells at other anatomical sites. Interestingly, commercially sourced recombinant CCN3 did not induce oligodendrocyte differentiation (data not shown). This may be due to the lack of critical post-translational modifications in recombinant CCN3 and/or the presence of a 10-His tag at the C-terminus of the recombinant protein. This tag may impair bioactivity of this key functional region of CCN3, which contains a cysteine knot motif involved in homo- and heterodimerization. This emphasizes the importance of both gain-of-function and loss-of-function studies of CCN3 in reductionist and more complex models.

Recently Burzyn *et al.* identified roles for Treg in muscle regeneration associated with local immunomodulation and amphiregulin expression[9] while Arpaia *et al*. reported TCR-independent tissue protective functions of amphiregulin-expressing Treg in influenza-infected lungs[10]. Other studies described associations of Treg with regeneration of cardiac muscle and neurons[31-33]. Here,

we identified that Treg directly promote oligodendrocyte differentiation and myelin production even in the absence of overt inflammation. Thus, signaling from Treg can directly increase the regenerative capacity of a progenitor cell population, independent of immunomodulation known to support regeneration at other anatomical sites. This confers a primary regenerative role for Treg complementary to, but distinct from, known immunomodulatory functions. In concert, these two functions confer fundamental damage-limiting and damage-resolving roles to Treg. Therapies to boost tissue regeneration should consider this emerging and central role of Treg in natural regeneration. This knowledge holds therapeutic potential for tissue regeneration in diseases such as MS.

Collectively, our novel findings and recent studies by others show that Treg promote regeneration via different factors in different tissues. Our regenerative immunology study expands the classical functions of T-reg beyond reg-ulation to reg-eneration.

## Online methods

### Animals

All mice were on a C57BL/6 background and were bred in-house. Foxp3-DTR mice were a kind gift from Prof. Alexander Rudensky (Memorial Sloan Kettering Institute, New York) and Foxp3-eGFP mice were a kind gift from Prof. B. Malissen[34]. Experiments used both male and female neonatal P0-P9 pups and animals from 6-16 weeks from sources above. To deplete $Foxp3^+$ cells in Foxp3-DTR mice, diphtheria toxin was administered as described below. All animal maintenance and experiments were in compliance with the UK Home Office and approved by the University's Ethical Committee.

### Treg depletion and induction of lysolecithin-mediated demyelination

To deplete $Foxp3^+$ cells in Foxp3-DTR mice 1 μg DT in 200 μl saline was injected i.p. daily for 3-4 days before demyelination. For maintenance of Treg depletion, 1 μg DT was injected i.p. every 3$^{rd}$ day after the demyelination procedure. Control mice were treated with saline. Depletion was routinely confirmed in blood and spleen by flow cytometry. L-α-Lysophosphatidylcholine (lysolecithin) was used to induce a focal demyelinated lesion in the spinal cord of mice as described previously[6,35]. In brief, 1.2 μl lysolecithin (Sigma) was injected into the ventral white matter of the lower thoracic spinal cord between vertebrae T11-12 or T12-13. At indicated time points, mice were terminally anesthetized with Ketamin/Rompun, transcardially perfused with 4% paraformaldehyde in PBS or PBS alone (for flow cytometry studies), and spinal cord tissue was dissected.

### Adoptive transfer of wild-type Treg into Treg-depleted FoxP3-DTR mice

FoxP3-DTR mice were treated with DT as described above. In the 24 hr prior to lysolecithin-induced demyelination, mice were injected i.p. with $1x10^6$ MACS-purified Treg from wild-type mice that were insensitive to DT treatment.

### Tissue processing

For immunohistochemistry, spinal cord tissue was post-fixed for 2-4 hr in 4% PFA and immersed in 20% sucrose in PBS solution overnight. For cryo-preservation spinal cords were embedded with OCT medium (VWR) and non-consecutive 12 µm thick cryo-sections from the approximate center of lesions were mounted on glass slides[4].

**Immunofluorescence staining of CNS tissue**

After blocking with 10% goat serum, spinal cord sections were incubated with antibodies for APC (1:100, clone CC1, Abcam), Ki67 (1:200, clone SoIA15, eBioscience), and Olig2 (1:200; cat. no. AB9610, Millipore) overnight. Secondary antibodies goat anti-rabbit AF488 (1:200; cat. no. A-11008, Life Technologies) and goat anti-rat AF594 (1:200; cat. no. A-11007, Life Technologies) were incubated for 1 hr at RT. For CC1 detection acidic antigen retrieval was performed and a mouse-on-mouse immunodetection kit was used (Vector Laboratories). Nuclei were counterstained with DAPI before coverslipping with ProLong Gold Antifade (Life Technologies). Spinal cord images were acquired on a Leica DM5500 epifluorescence microscope.

**Luxol Fast Blue staining of spinal cord tissue**

Tissue was placed in 1:1 alcohol:chloroform solution for 10 hr before dehydration in alcohol and incubation in 0.1% luxol fast blue solution (Sigma) at 56°C for 16 hr. Tissue was rinsed and differentiated in 0.05% lithium carbonate solution for 30 sec followed by 70% alcohol for 30 sec. After washing with distilled water tissue was differentiated in 95% alcohol and twice in 100% alcohol (each 5 min) before immersing twice in xylene for 5 min and coverslipping.

**Electron Microscopy of spinal cord lesions**

Animals were perfused with 3% glutaraldehyde, 2% paraformaldehyde, 0.1M phosphate buffer (pH 7.4), 0.7% (w/v) NaCl and spinal cords were dissected and post-fixed overnight. Specimen were post-fixed in 1% osmium tetraoxide (Agar Scientific, Stansted, UK), dehydrated, stained en bloc with

uranyl acetate (Agar Scientific, Stansted, UK), and embedded in Durcupan resin (Sigma-Aldrich, UK). Ultrathin sections (70 nm) were cut on a Leica UCT ultramicrotome with a Diamond knife (Diatome), mounted on formvar-coated copper grids (Electron Microscopy Science), and counterstained with uranyl acetate and lead citrate. Random electron micrographs (35 per animal) were taken from the lesions with a FEI Spirit transmission microscope with a Gatan Orius SC200B Camera. A total of 3399 control axons and 2076 axons from Treg-depleted lesions were analysed blindly.

**Flow cytometric immunophenotyping**

Fresh spinal cord tissue was dissected following transcardial perfusion with PBS was weighed and placed in Neuro Medium (Miltenyi Biotec). Medium was removed and tissues were individually passed through 70 µm strainers, washed with 30% percoll to pellet cells and myelin-containing supernatant was carefully removed. Cells were resuspended in 200 µl flow cytometry staining buffer (FCSB; 1% FCS, 0.01% $NaN_3$ in PBS) prior to cell surface staining with antibodies to CD45 (clone 104), CD11b (clone M1/70), CD3 (clone 145-2C11) and CD4 (clone GK1.5). Foxp3 expression was determined in fresh cells from Foxp3-eGFP or Foxp3-GFP-DTR mice. To calculate cell numbers, singlets were identified by FSC-H vs FSC-A, and $CD45^+$ cells were gated for subsequent analyses of CD11b, CD3, CD4 and Foxp3-eGFP. All flow cytometry antibodies were from eBioscience. Data were acquired on a FACSCanto II and analyzed using FlowJo software.

**Cuprizone-induced demyelination**

Eleven-week-old male C57BL/6 and FoxP3DTR mice were fed with 0.2% cuprizone [bis(cyclohexanone) oxaldihydrazone, (Teklad Costum Diet TD.140804, Envigo]. Food and water were available *ad libitum*. Cuprizone feeding was maintained for 25 days to induce demyelination. Diet was then changed to normal rodent chow for additional 2 weeks to allow remyelination to occur. To deplete Treg, mice were injected with DT (0.04g DT/Kg) or vehicle on day 24 and day 25.

Treg depletion was maintained by DT administration every three days. Mice were sacrificed on day 39 and were perfused transcardially with PBS followed by cold 4% paraformaldehyde. Brains were removed, postfixed overnight in 4% paraformaldehyde and cryoprotected in 30% sucrose. Coronal frozen sections of 20 µm thickness were cut using a Leica cryostat. Sections between 1 mm and -1 mm relative to Bregma were collected and stained for CC1 and Olig2 as described above. The number of mature oligodendrocytes in the corpus callosum was quantified on images of 1-2 sections per animal with five animals per group. Images of the midline segment of the corpus callosum from frontal and middle sections were used to delineate the area for analysis of Olig2/CC1 positive cells.

**Black Gold II staining**

Tissue sections were stained with Black Gold II (AG105, Millipore Corp, Billerica, MA) according to manufacturer's instructions. Briefly, sections were washed in water, immersed in pre-warmed Black Gold II solution and incubated at 60°C for 15 min followed by transfer into pre-warmed 1% sodium thiosulfate at 60°C for 5 min. Slides were rinsed three times, dehydrated, immersed in xylene for 2 min and coverslipped with mounting media.

**Gene expression analyses**

For qPCR, total RNA was extracted from the cerebella of perfused mice with an RNeasy FFPE kit (Qiagen) using a modified protocol. Tissue was homogenised in supplied PKD buffer before treatment with proteinase K. All subsequent steps were followed according to manufacturer's instructions. RNA purity and concentration was assessed by Nanodrop spectrophotometry. Samples were treated with DNase I (Invitrogen) prior to reverse transcription with Superscript IV (Invitrogen). cDNA samples were assayed in triplicate by qPCR using Fast SYBR Green (ThermoFisher Scientific) on a Roche LightCycler 480 system. Relative gene expression of *plp1* gene was determined with the

Pfaffl method using *gapdh* as internal control[36] . Primer sequences were as previously described[37]. An unpaired, two-tailed Student's t test was performed to assess statistical differences on delta Ct values of each condition, with a significance threshold of 0.05.

*In situ* hybridization of proteolipid protein (PLP) on paraformaldehyde-fixed CNS tissue was performed as previously described[38]. The plasmid containing a fragment of 801bp plp cDNA was provided by Prof I Griffith (University of Glasgow). Briefly, sections were incubated with digoxigenin-labeled complementary RNA probes at 65°C overnight and subjected to a standard wash protocol (50% formamide, 1× standard saline citrate, 0.1% Tween-20, 65°C, 3× 30 minutes) to remove nonspecific probe binding. The target bound probes were detected by alkaline phosphatase–conjugated antidigoxigenin antibody, and visualized as purple precipitate after incubation in NBT/BCIP solution according to the manufacturer's instructions (Roche, Lewes, UK). The slides were dehydrated with ascending concentration of ethanol, cleared with xylene, and mounted in dibutyl phthalate in xylene. Images were acquired with the Zeiss Axio Observer microscope.

**T cell culture**

$CD4^+$ T cells were immunomagnetically purified by negative selection (Stem Cell Technologies) from splenocytes of 6-10 week old female C57BL/6 mice and cultured in RPMI 1640 (Life Technologies) supplemented with 10% FCS, 1% penicillin/streptomycin, 1% L-glutamine, 1% Hepes, 1% sodium pyruvate, 1% non-essential amino acids and 50 nM β-mercaptoethanol. In Supplementary Fig 3d, naïve $CD4^+$ T cells were purified using EasySep™ Mouse Naïve $CD4^+$ T Cell Isolation Kits (Stem Cell Technologies). T cells were activated with plate bound anti-CD3 (1 µg/ml, clone 145-2C11) and soluble anti-CD28 (1 µg/ml, clone 37.51) (both eBioscience) for 3 days in non-polarizing (NP; no exogenous cytokine) or Treg-polarizing conditions consisting of rhTGF-β (2 ng/ml, R&D Systems), rhIL-2 (10 ng/ml, eBioscience) and anti-IFN-γ (10 µg/ml, clone XMG1.2, Bioxcell). T cells were then reactivated in brain slice medium (described below) for a further 72 hr and conditioned media were harvested. Polarization of all cultures was verified by flow cytometry and Treg cultures used for

experiments generally consisted of 80-90% Foxp3$^+$ T cells (see Supplementary Fig. 2 f). For CCN3 immunoblotting, depletion and elution, cells were reactivated in serum-free X-VIVO15 medium (Lonza).

For adoptive transfer experiments, nTreg were immunomagnetically purified (Stem Cell Technologies) by negative selection of CD4$^+$ T cells followed by positive selection of CD25$^+$ cells from splenocytes and lymph nodes of C57BL/6 mice. For i.p. injection cells were resuspended at 5x10$^6$ cells/ml in saline.

**Organotypic brain slice culture**

Brain stem slices (300 µm) from P0-2 C57BL/6 pups were prepared using a Mcllwain Tissue Chopper and cultured in transwell inserts with brain slice medium consisting of 46.6% minimum essential medium, 25% Earle's balanced salt solution, 25% heat inactivated horse serum, 1% penicillin/streptomycin, 1% glutamax (Life Technologies) and 1.4% D-glucose (Sigma). Where indicated, slices were treated with 5% T cell-conditioned media and/or anti-CCN3 (10 µg/ml; clone 231216, R&D Systems) and/or isotype control (clone 54447, R&D Systems) every other day. For remyelination studies, brain stem slices were demyelinated after 14 days in culture with lysolecithin (0.5 mg/ml, Sigma) for 16 hr. Slices were washed and allowed to remyelinate for up to 14 days. For co-culture studies, 1.7x10$^4$ FACS-purified natural Treg from Foxp3-eGFP mice were added directly on to brain stem slices in a volume of 10 µl (Supplementary Fig. 2 a).

**Staining of organotypic brain slices**

Slices were fluorescently stained for myelin basic protein (MBP; 1:600, clone 12, Millipore) and axonal neurofilament-200 (NF200; 1:200, clone RT97, Millipore). After fixation in 4% paraformaldehyde for 45 min at RT, slices were blocked and permeabilized at RT for 1 hr in 3% heat-inactivated horse serum (Life Technologies), 2% bovine serum albumin (Sigma) and 0.5% Triton X-100 (Sigma). Both primary and secondary antibodies (goat anti-rat AF594, cat. no. A11007, goat anti-

mouse AF488 cat # A11001 and goat anti-mouse AF405 cat # A31553, 1:500; Life Technologies) were incubated overnight at 4°C. Slices were mounted with ProLong Gold Antifade (Life Technologies) and imaged with a Leica TCS SP5 confocal microscope at 0.5 µm intervals over 10 µm, taking up to 5 fields of view (FOV) per slice, dependent on slice size. Representative images were displayed with a green look up table (LUT) for NF200 and red LUT for MBP, applied using Leica AF software.

**Electron microscopy of organotypic brain slices**

Slices were immersion fixed in 4%PFA/2% glutaraldehyde in 0.1M phosphate buffer for 24 hr, washed in phosphate buffer and post-fixed in 1% osmium tetroxide in 0.1 M phosphate buffer for 45 min. Samples were dehydrated in increasing concentrations of acetone and embedded in Araldite resin. Ultrathin 60 nm sections were stained in uranyl acetate and lead citrate and then viewed in a JEM1400 Transmission electron microscope (JEOL). To count the percentage of myelinated fibres per unit area of slice (at least 600 $\mu m^2$/condition), three photographs were taken from random, non-overlapping fields from each of 3 slices per condition and analysed. To measure g-ratios, at least 35 randomly chosen axons from each of 3 slices per condition were analysed by tracing the axonal circumference and the whole fibre circumference (using a graphics pad and pen). G-ratios were calculated by dividing these values and data were analysed using one-way ANOVA with Bonferroni post-test with $p < 0.05$ considered significant.

**Mixed glial cultures**

Mixed glial cells were generated from P2-7 C57BL/6 pups according to the protocol of the Neural Tissue Dissociation Kit (P) (Miltenyi Biotec). In short, brains were dissected, cerebellum and meninges were removed and tissue was dissociated via mechanical and papain enzyme digestion prior to filtration through a 40 µm strainer. Cells were plated in poly-L-lysine-coated (10 µg/ml, Sigma) 96 well flat, glass-bottomed plates (BD Falcon) at a density of $10^5$ cells per well and cultures were maintained at 37˚C, 5% $CO_2$. Cells were cultured for 5 days in DMEM (Life Technologies)

supplemented with PDGFαα (10 ng/ml; PeproTech), 10% endotoxin-free FCS, 1% penicillin/streptomycin and 1% L-glutamine (Life Technologies). Cells were cultured for a further 2 days in neural medium (Miltenyi Biotec) supplemented with 1% penicillin/streptomycin, 1% L-glutamine, 2% B27/MACS Neuro Brew21 (Miltenyi Biotec) and PDGFαα (10 ng/ml; PeproTech). At day 7 in culture, PDGFαα was withdrawn to allow oligodendrocyte differentiation and cells were stimulated with 5% Treg-conditioned media, rCCN3, anti-CCN3 (clone 231216) or isotype control (clone 54447) (all R&D Systems) or controls for up to 5 days.

**Immunofluorescence staining of mixed glial cultures**

Cell cultures were fixed in 4% paraformaldehyde (pH 7.4) for 15-20 min at RT and blocked in 10% normal goat serum with 0.1% Triton-X-100 for 1 hr. Cells were then incubated with primary antibody overnight at 4˚C and in secondary antibodies for 1 hr at RT. Cells were counterstained with DAPI for 5 min at RT. Primary antibodies used were rabbit anti-mouse Olig2 (1:200; cat. no. AB9610, Millipore), rat anti-mouse MBP (1:200; clone 12, Millipore), rat anti-mouse Ki67 (1:200; clone SoIA15, eBioscience), rabbit anti-mouse GFAP (1:200; cat. no. Z0334, Dako) and rat anti-mouse CD11b (1:200; clone M1/70, eBioscience) and secondary antibodies used were goat anti-rabbit AF488 (1:1000; cat. no. A-11008) and goat anti-rat AF594 (1:1000; cat. no. A-11007; both Life Technologies). For live/dead staining unfixed cells were stained using the LIVE/DEAD® Viability/Cytotoxicity Kit for mammalian cells (Life Technologies). Immunofluorescence was detected using an EVOS microscope at 10X magnification and n=6 wells per condition with one mean value from multiple images calculated for each well.

**OPC purification**

Immunopanning purification of OPC was performed as previously described[39]. Briefly, OPC were purified from P7–9 mouse brain cortices. Tissue culture dishes were incubated overnight with goat

IgG and IgM secondary antibodies to mouse (cat. no. 115-005-004, Jackson Laboratories) in 50 mM Tris-HCl at a final concentration of 10 µg/ml, pH 9.5. Dishes were rinsed and incubated at room temperature (RT) with primary antibodies for Ran-2, GalC and O4 from hybridoma supernatants[39]. Rodent brain hemispheres were diced and dissociated with papain (Worthington) at 37°C. After trituration, cells were resuspended in a panning buffer (0.2% BSA in DPBS) and incubated at RT sequentially on three immunopanning dishes: Ran-2 and GalC were used for negative selection before positive selection with O4. OPC were released from the final panning dish using 0.05% Trypsin (Invitrogen). OPCs were typically 95% pure after immunopanning, with a viability of 94%.

**OPC–DRG co-cultures**

OPC-DRG co-cultures were prepared as previously described[39]. Briefly, DRG neurons from E15 Sprague-Dawley rats were dissociated, plated (150,000 cells per 25 mm cover glass) and purified on collagen-coated coverslips in the presence of 100 ng/ml NGF (AbD Serotec). Neurons were maintained for 3 weeks and washed with DMEM (Invitrogen) extensively to remove any residual NGF before seeding OPC. Co-cultures were grown in chemically defined medium composed of DMEM (Invitrogen) supplemented with B27 (Invitrogen), N2 (Invitrogen), penicillin-streptomycin (Invitrogen), N-acetyl-cysteine (Sigma-Aldrich) and forskolin (Sigma-Aldrich).

**CCN3 quantification and depletion**

Proteome profiling of conditioned media was performed using an Angiogenesis Antibody Array (R&D Systems) as per manufacturer's instructions, which identified CCN3 as a candidate protein of interest. Levels of CCN3 in T cell-conditioned media were quantified by ELISA (R&D Systems) according to manufacturer's instructions.

Treg-conditioned media were depleted of CCN3 using monoclonal anti-CCN3 antibody-coupled magnetic beads (clone 231216, R&D Systems and Thermo Scientific) or isotype control-coupled beads (clone 54447). Coupling of antibody and beads was performed according to manufacturer's

instructions. In short, 1 mg of beads was incubated with 500 µg/mL of antibody solution and the flow-through was analysed by spectrophotometry. For immunoprecipitation, up to 1 ml of Treg-conditioned media were added to 1 mg of monoclonal antibody-coupled magnetic beads and incubated on a rotator at RT for 2 hr with additional vortexing of the samples every 15 min to ensure that the beads remained in suspension. The samples were then placed in a magnetic stand and CCN3-depleted Treg-conditioned media and isotype-treated controls were collected. To elute Treg-derived CCN3, beads were washed and elution buffer (0.1 M glycine, pH 2.0) was added for 3-5 min at RT. To neutralize the low pH of the solution, neutralization buffer (1 M Tris, pH 7.4) was immediately added, samples were placed on a magnetic stand, and the eluate containing Treg-derived CCN3 was collected and resuspended in medium according to initial volume.

**Immunoblotting of CCN3**

T cell-conditioned media or recombinant CCN3 (R&D Systems) were enriched for CCN3 using heparin-sepharose beads as previously described[40]. In short, up to 10 ml of Treg-conditioned media (equivalent to 25 ng of CCN3), or recombinant CCN3 were added to 100 µl 50% heparin-sepharose slurry and incubated on a rotator at 4°C overnight. 50 µl of PBS-washed CCN3-bound heparin-sepharose beads and 12.5 µl 5x reducing loading dye were boiled for 10 min prior to loading on a reducing 15% SDS-PAGE. Following transfer onto PVDF membrane (Millipore) and blocking (3% BSA in PBS/1% Tween) for 1 hr at RT, protein was probed using polyclonal anti-CCN3 antibody (1:1000; cat. no. AF1976, R&D Systems) overnight at 4$^{o}$C and secondary anti-goat HRP (1:3000; cat. no. sc-2020, Santa Cruz) for 1 hr at RT.

**Image analysis and data processing**

Customized ImageJ[41] plugins were used to assist quantifying positively stained cells and areas in all models.

Regions of interest corresponding to spinal cord lesions were initially drawn using the polygon tool. Regions were subsequently refined based on the local cell density by thresholding a Gaussian-smoothed duplicate of the DAPI channel to give a more detailed contour which was corrected manually if necessary using a brush selection tool. Cells were then counted manually within the lesion; in some cases counts were automatically initialized as localized regions of high fluorescence detected by the 'find maxima' command of ImageJ before manual verification and correction to ensure that all regions contributing to the final counts were consistent with expected cell morphology (i.e. no artefacts). ImageJ plugins were written to perform the lesion refinement and to assist with manual cell counting.

Myelination index was used for overlap of myelin and axonal markers in 3D, indicating (re)myelination. Confocal z-stacks of brain slices, both red (MBP) and green (NF200) channels were pre-processed by first smoothing with a 3D isotropic Gaussian filter (sigma = 0.5 µm) before subtracting a background estimate created by applying a 3D morphological opening (filter radius = 1 µm). The processed channels were then thresholded, where the threshold was determined automatically by implementation of the 'triangle' method of ImageJ. The overlap coefficient was determined as the proportion of above-threshold pixels in the green channel that were also detected in the red channel, which quantified MBP signals co-localizing with NF200 signals. An ImageJ plugin was written to fully automate the above steps. $MBP^+$ oligodendrocytes were counted manually.

Cell counts of $Olig2^+$, $MBP^+$ and $Ki67^+$ cells in mixed glial cultures were performed manually. $MBP^+$ areas were determined from the number of above-threshold pixels after applying a small median filter (radius = 1.5 pixels), followed by subtracting a background image generated by the 'subtract background' command of ImageJ (sliding paraboloid option, radius = 100 pixels). For each plate the threshold was determined and the same threshold was applied to all analyzed images within each experiment. An ImageJ plugin was written to automate the above steps. Plugin codes will be made publically available on the Queen's University Belfast website.

**Experimental designs and statistical analyses**

In all models, sample sizes were chosen based on studies reported previously. For *in vivo* studies, any animal that reached a pre-defined welfare limit before the analysis time-point was excluded from the study. For organotypic brain slice experiments, slice integrity was determined by neurofilament 200 staining prior to analysis. Animals and brain slices were randomly assigned to experimental groups at the beginning of experiments. For certain *in vivo* experiments, image assessment was blinded by generating randomized file names prior to analysis (see code availability section below). Myelination indices (brain slices) and MBP area (glial cultures) were blindly assessed by a computer programme and in an identical manner for all files. Datasets were tested for normal distribution, variances and statistical significance using unpaired, two-tailed, Student's *t* tests for parametric data with or without Welch correction, or Mann-Whitney tests for non-parametric data, detailed in legends. All statistical analysis and graphing of data were performed using GraphPad Prism.

**Data and code availability**

The datasets generated during and/or analysed during the current study are available from the corresponding author on reasonable request. All randomization and analysis coding can be downloaded freely at: http://tinyurl.com/QUBFitzgeraldGroup-FreeToShare

**Author contributions**

Experiments were designed, performed and analyzed by YD, TOH, MD, RP, SRM, SF, MN, GE, JM, JF, IVA, JRC and DCF. Image analysis tools were developed by PB and PH. EM was performed by EE, AB and AW. CZ, RH, AK, PM, BP, RJI, JRC and RJMF provided advice on experimental design and interpretation, and IVA, PM and RJMF provided mentorship. Manuscript was written by YD and DCF with contributions from all authors. DCF oversaw the study.

**Acknowledgments**

We thank Prof. A. Rudensky for providing Foxp3-DTR mice and Prof. B. Malissen for the provision of Foxp3-eGFP mice. We acknowledge extensive technical support from Suzanne Leech, Shannon Peoples, Nira de la Vega Gallardo, Steve Mitchell, Joanna Brown, Raphael Blain and the staff of the animal facility. This work was supported by the Biotechnology and Biological Sciences Research Council (DF), Department of Employment and Learning (DF), The Leverhulme Trust (YD and DF), The UK Multiple Sclerosis Society (RF and CZ) and the British Neuropathology Society (YD and DF), The Wellcome Trust (DF) and the University of Edinburgh Wellcome Trust Multi User Equipment Grant (WT104915MA).

## References


1. Funfschilling, U*., et al.* Glycolytic oligodendrocytes maintain myelin and long-term axonal integrity. *Nature* **485**, 517-521 (2012).

2. Lee, Y*., et al.* Oligodendroglia metabolically support axons and contribute to neurodegeneration. *Nature* **487**, 443-448 (2012).

3. Miron, V.E*., et al.* M2 microglia and macrophages drive oligodendrocyte differentiation during CNS remyelination. *Nat Neurosci* **16**, 1211-1218 (2013).

4. Ruckh, J.M*., et al.* Rejuvenation of regeneration in the aging central nervous system. *Cell Stem Cell* **10**, 96-103 (2012).

5. Bieber, A.J., Kerr, S. & Rodriguez, M. Efficient central nervous system remyelination requires T cells. *Ann Neurol* **53**, 680-684 (2003).

6. Woodruff, R.H., Fruttiger, M., Richardson, W.D. & Franklin, R.J. Platelet-derived growth factor regulates oligodendrocyte progenitor numbers in adult CNS and their response following CNS demyelination. *Mol Cell Neurosci* **25**, 252-262 (2004).

7. Arnett, H.A*., et al.* bHLH transcription factor Olig1 is required to repair demyelinated lesions in the CNS. *Science* **306**, 2111-2115 (2004).

8. Ousman, S.S. & David, S. Lysophosphatidylcholine induces rapid recruitment and activation of macrophages in the adult mouse spinal cord. *Glia* **30**, 92-104 (2000).

9. Burzyn, D*., et al.* A special population of regulatory T cells potentiates muscle repair. *Cell* **155**, 1282-1295 (2013).

10. Arpaia, N*., et al.* A Distinct Function of Regulatory T Cells in Tissue Protection. *Cell* **162**, 1078-1089 (2015).

11. Kim, J.M., Rasmussen, J.P. & Rudensky, A.Y. Regulatory T cells prevent catastrophic autoimmunity throughout the lifespan of mice. *Nat Immunol* **8**, 191-197 (2007).

12. Christiaansen, A.F., Boggiatto, P.M. & Varga, S.M. Limitations of Foxp3(+) Treg depletion following viral infection in DEREG mice. *J Immunol Methods* **406**, 58-65 (2014).

13. Meyer Zu Horste, G*., et al.* Active immunization induces toxicity of diphtheria toxin in diphtheria resistant mice--implications for neuroinflammatory models. *J Immunol Methods* **354**, 80-84 (2010).

14. Mayer, C.T*., et al.* Advantages of Foxp3(+) regulatory T cell depletion using DEREG mice. *Immun Inflamm Dis* **2**, 162-165 (2014).

15. Huang, J.K*., et al.* Retinoid X receptor gamma signaling accelerates CNS remyelination. *Nat Neurosci* **14**, 45-53 (2011).

16. Zhang, H., Jarjour, A.A., Boyd, A. & Williams, A. Central nervous system remyelination in culture--a tool for multiple sclerosis research. *Exp Neurol* **230**, 138-148 (2011).

17. Hild, W. [Myelin formation in central nervous system tissue cultures]. *Verh Anat Ges* **53**, 315-317 (1956).

18. Birgbauer, E., Rao, T.S. & Webb, M. Lysolecithin induces demyelination in vitro in a cerebellar slice culture system. *J Neurosci Res* **78**, 157-166 (2004).

19. Ling, C., Verbny, Y.I., Banks, M.I., Sandor, M. & Fabry, Z. In situ activation of antigen-specific CD8+ T cells in the presence of antigen in organotypic brain slices. *J Immunol* **180**, 8393-8399 (2008).

20. Kim, J.*, et al.* PINK1 Deficiency Enhances Inflammatory Cytokine Release from Acutely Prepared Brain Slices. *Exp Neurobiol* **22**, 38-44 (2013).

21. Sheridan, G.K. & Dev, K.K. S1P1 receptor subtype inhibits demyelination and regulates chemokine release in cerebellar slice cultures. *Glia* **60**, 382-392 (2012).

22. Su, B.Y.*, et al.* The expression of ccn3 (nov) RNA and protein in the rat central nervous system is developmentally regulated. *Mol Pathol* **54**, 184-191 (2001).

23. Leask, A. & Abraham, D.J. All in the CCN family: essential matricellular signaling modulators emerge from the bunker. *J Cell Sci* **119**, 4803-4810 (2006).

24. Lin, C.G.*, et al.* CCN3 (NOV) is a novel angiogenic regulator of the CCN protein family. *J Biol Chem* **278**, 24200-24208 (2003).

25. Wang, X., He, H., Wu, X., Hu, J. & Tan, Y. Promotion of dentin regeneration via CCN3 modulation on Notch and BMP signaling pathways. *Biomaterials* **35**, 2720-2729 (2014).

26. Kotter, M.R., Setzu, A., Sim, F.J., Van Rooijen, N. & Franklin, R.J. Macrophage depletion impairs oligodendrocyte remyelination following lysolecithin-induced demyelination. *Glia* **35**, 204-212 (2001).

27. Perbal, B. NOV (nephroblastoma overexpressed) and the CCN family of genes: structural and functional issues. *Mol Pathol* **54**, 57-79 (2001).

28. Perbal, B. CCN proteins: A centralized communication network. *J Cell Commun Signal* **7**, 169-177 (2013).

29. Le Dreau, G.*, et al.* NOV/CCN3 promotes maturation of cerebellar granule neuron precursors. *Mol Cell Neurosci* **43**, 60-71 (2010).

30. Xin, L.W., Martinerie, C., Zumkeller, W., Westphal, M. & Perbal, B. Differential expression of novH and CTGF in human glioma cell lines. *Clin Mol Pathol* **49**, M91-97 (1996).

31. Raposo, C.*, et al.* CNS repair requires both effector and regulatory T cells with distinct temporal and spatial profiles. *J Neurosci* **34**, 10141-10155 (2014).

32. Saxena, A.*, et al.* Regulatory T cells are recruited in the infarcted mouse myocardium and may modulate fibroblast phenotype and function. *Am J Physiol Heart Circ Physiol* **307**, H1233-1242 (2014).

33. Weirather, J.*, et al.* Foxp3+ CD4+ T cells improve healing after myocardial infarction by modulating monocyte/macrophage differentiation. *Circ Res* **115**, 55-67 (2014).

34. Wang, Y.*, et al.* Th2 lymphoproliferative disorder of LatY136F mutant mice unfolds independently of TCR-MHC engagement and is insensitive to the action of Foxp3+ regulatory T cells. *J Immunol* **180**, 1565-1575 (2008).

35. Hall, S.M. The effect of injections of lysophosphatidyl choline into white matter of the adult mouse spinal cord. *J Cell Sci* **10**, 535-546 (1972).

36. Pfaffl, M.W. A new mathematical model for relative quantification in real-time RT-PCR. *Nucleic Acids Res* **29**, e45 (2001).

37. Liu, J.*, et al.* Impaired adult myelination in the prefrontal cortex of socially isolated mice. *Nat Neurosci* **15**, 1621-1623 (2012).

38. Zhao, C., Li, W.W. & Franklin, R.J. Differences in the early inflammatory responses to toxin-induced demyelination are associated with the age-related decline in CNS remyelination. *Neurobiol Aging* **27**, 1298-1307 (2006).

39. Mei, F.*, et al.* Micropillar arrays as a high-throughput screening platform for therapeutics in multiple sclerosis. *Nat Med* **20**, 954-960 (2014).

40. Chevalier, G.*, et al.* novH: differential expression in developing kidney and Wilm's tumors. *Am J Pathol* **152**, 1563-1575 (1998).

41. Schneider, C.A., Rasband, W.S. & Eliceiri, K.W. NIH Image to ImageJ: 25 years of image analysis. *Nat Methods* **9**, 671-675 (2012).

**Figure 1.** **Treg are required for efficient OPC differentiation during remyelination**

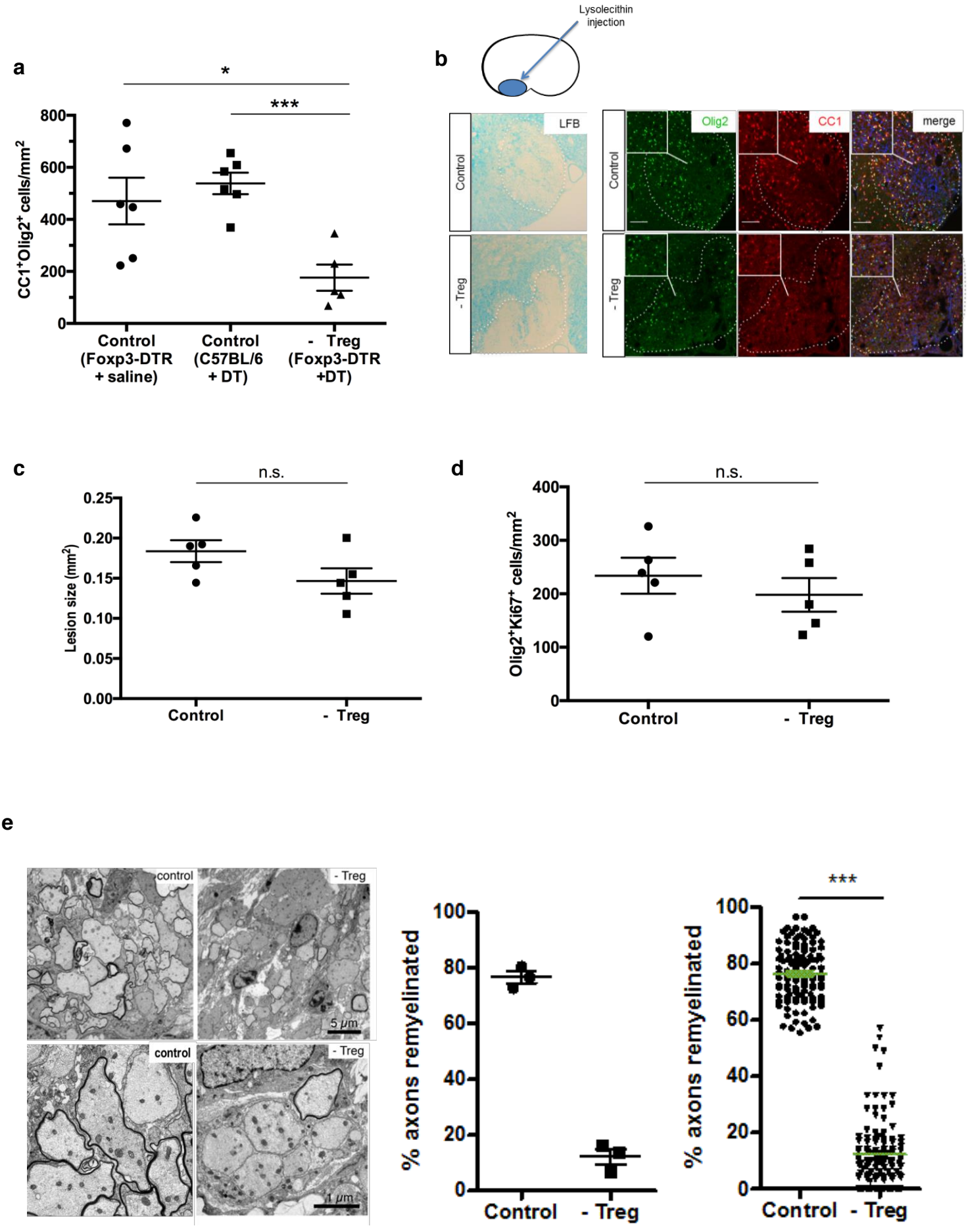

**Figure 1.** **Treg are required for efficient OPC differentiation during remyelination**

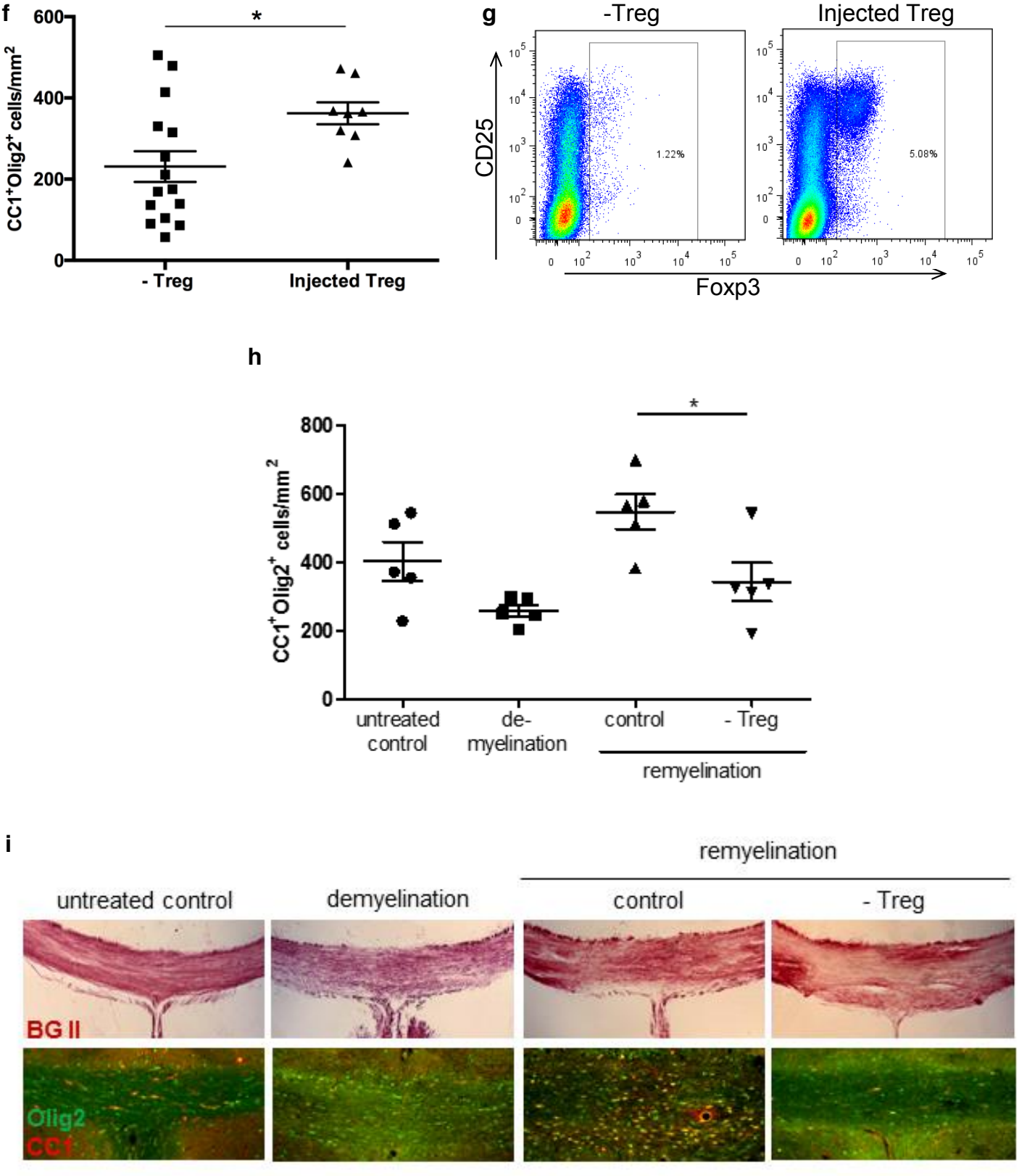

**Figure 1. Treg are required for efficient OPC differentiation during remyelination**

C57BL/6 and Foxp3-DTR mice were treated with diphtheria toxin (DT) to deplete $Foxp3^+$ Treg or saline as a control. **(a-g)** A focal demyelinated lesion was induced with lysolecithin on day 0 or **(h,i)** demyelination was induced by cuprizone feeding. In **(f,g)** Treg were MACS-purified from wildtype mice and $10^6$ cells/mouse were injected i.p. in the 24 hr prior to spinal cord lesioning of Treg-depleted mice (Foxp3-DTR+DT). For immunohistochemistry, tissues were fixed by transcardial perfusion and cryosections were stained for oligodendrocyte (Olig2, CC1), proliferation (Ki67) markers and counter-stained with DAPI (blue). Cell numbers were manually counted and normalized to lesion area. EM was performed as described in methods.

**(a)** Immunohistochemical analysis of $CC1^+Olig2^+$ cells per lesion area of Foxp3-DTR and C57BL/6 mice at 14 d.p.l, with n=6 in control and n=5 in Treg-depleted groups.
**(b)** Representative images of **(a)** taken on a Leica DM5500 Epifluorescence microscope (scale bar=100 µm) (LFB=Luxol fast blue staining).
**(c)** Lesion size of Foxp3-DTR mice +/- DT at 5 d.p.l. n=5 animals per group.
**(d)** $Olig2^+Ki67^+$ cells per lesion area of Foxp3-DTR mice at 5 d.p.l. n=5 animals per group.
**(e)** Electron micrographs showing distribution of remyelinated axons versus unmyelinated axons in control or Treg-depleted lesions at 17 d.p.l. Scale bar 5 µm (top) and 1 µm (bottom). Fewer axons are remyelinated in Treg-depleted animals than in control animals. Three animals per group were analysed (middle panel). Data (right panel) represent mean ± SEM from 109 micrographs from 3 mice per group. Two-tailed Mann-Whitney test.
**(f)** $CC1^+Olig2^+$ cells per lesion area of Foxp3-DTR mice with or without adoptively transferred Treg at 14 d.p.l., with pooled n=15 animals in Treg-depleted, n=8 in Treg-depleted/adoptively transferred Treg group.
**(g)** Representative flow cytometric identification of adoptively transferred Treg in lymph nodes of Treg-injected mice from **(f)** and controls, gated on $CD4^+$ cells.
**(h)** Immunohistochemical analysis of $CC1^+Olig2^+$ cells per lesion area of the corpus callosum at 2 weeks post-cuprizone withdrawal. n=5 animals, data represent analysis of 1-2 regions of corpus callosum per animal.
**(i)** Representative images of **(h)** at 10x magnification (Leica DM5500). Top: Black Gold II (BG) myelin stain. Bottom: $CC1^+Olig2^+$ staining.

Data shown are representative of 4 **(a,b)**, 3 **(c,d)**, 2 **(f,g)** and 1 **(e, h, i)** independent biological experiments, mean +/- SEM, student's t-test, unless otherwise indicated. *p<0.05, ***p<0.001.

**Figure 2. Treg directly promote brain tissue myelination and remyelination *ex vivo.***

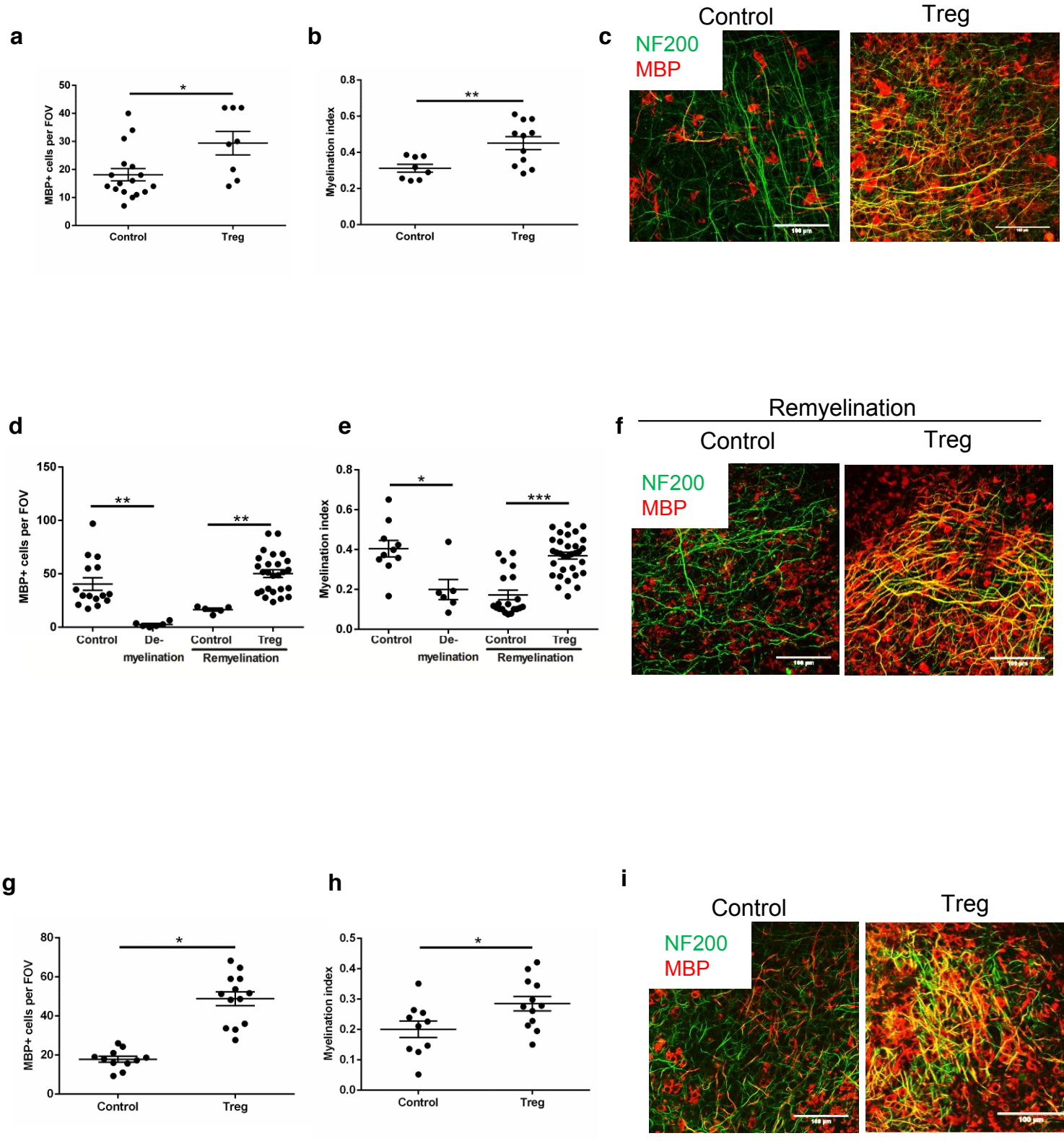

**Figure 2: Treg directly promote brain tissue myelination and remyelination *ex vivo***

Brain stem slices from P0-P2 mouse pups were cultured with Treg-conditioned media (Treg) or control media (control). In **(a-c)** brain slices were cultured for 7 days. In **(d-f)** brain slices were first cultured for 14 days prior to 16 hr of demyelination with lysolecithin. After lysolecithin removal, slices were cultured with Treg-conditioned media or control medium for an additional 7 days. In **(g-i)** brain slices were cultured for an initial 7 days after slicing and then with Treg-conditioned media or control medium for a further 7 days. Brain slices were stained for axonal (NF200) and myelin (MBP) markers. $MBP^+$ cells were manually counted and myelination index (myelin and axonal staining overlap, representing axonal ensheathment by myelin) was determined using an ImageJ plugin.

**(a-c)** Analysis of **(a)** $MBP^+$ cells and **(b)** myelination index per FOV. **(c)** Representative images taken from z-stacks at 7 d.i.v (scale bar=100 μm). Control n=17 and Treg n=8 fields of view from 3-4 slices/group, Student's t test.
**(d-f)** Analysis of **(d)** $MBP^+$ cells and **(e)** myelination index per FOV. **(f)** Representative images taken from z-stacks (scale bar=100 μm). Control n=10, demyelination n=6, remyelination control n=20 and Treg n=32 fields of view from 3-6 slices/group, Mann Whitney test.
**(g-i)** Analysis of **(g)** $MBP^+$ cells and **(h)** myelination index per FOV. **(i)** Representative images taken from z-stacks (scale bar=100 μm). Control n=11 and Treg n= 13 fields of view from 3-6 slices/group, Student's t test.

Data shown are representative of 6 **(a-c)** and 2 **(d-f, g-i)** independent experiments, mean +/- SEM, *p<0.05, **p<0.01, ***p<0.001.

**Figure 3. Treg directly enhance oligodendrocyte differentiation and myelination *in vitro.***

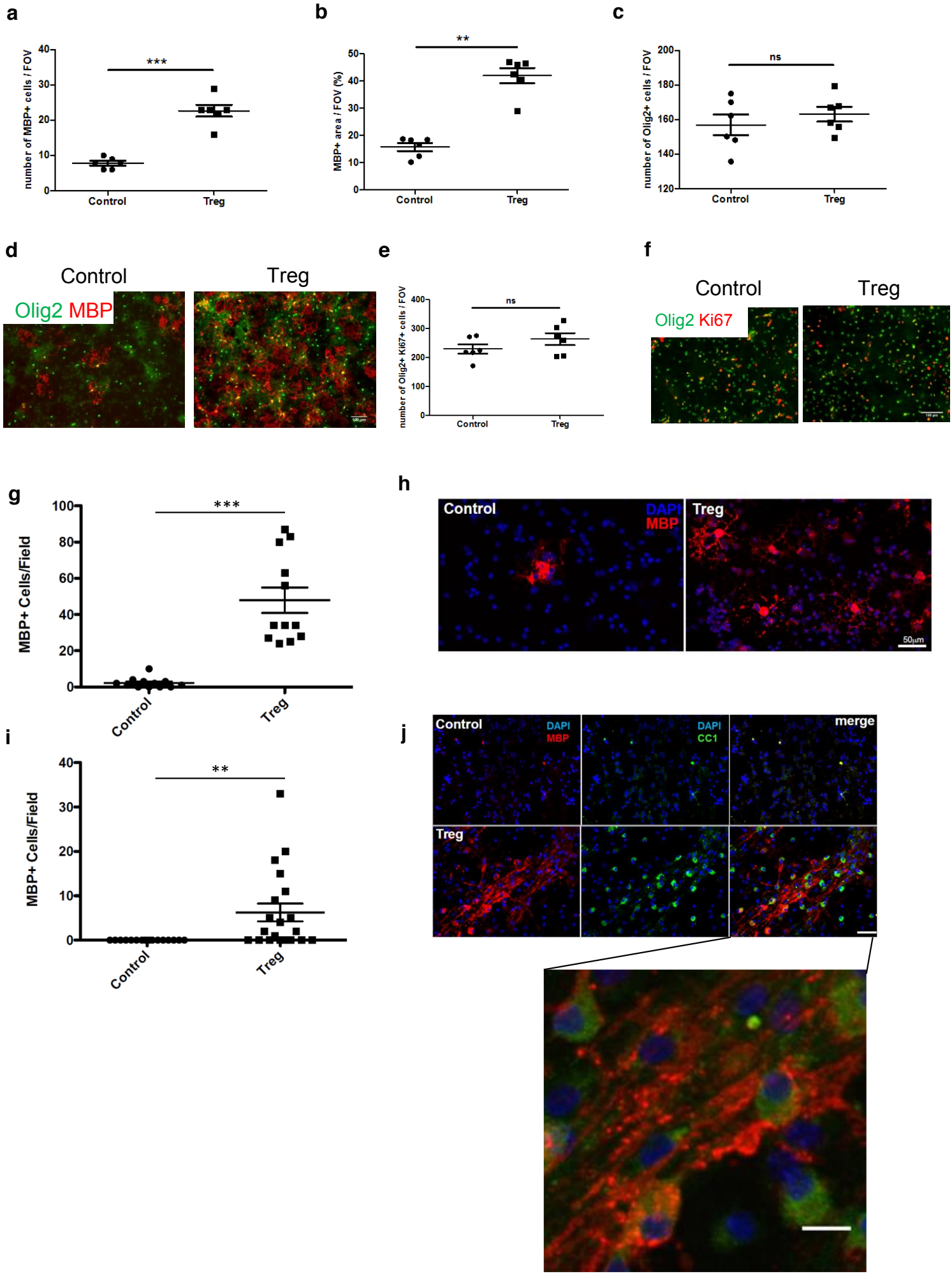

**Figure 3: Treg directly enhance oligodendrocyte differentiation and myelination *in vitro***

**(a-f)** Mixed glial cells from P2–7 mouse pup cortices were expanded for 7 days *in vitro* and then treated for **(a-d)** 5 or **(e,f)** 2 days with 5% Treg-conditioned media or control medium as indicated. Cells were stained for oligodendrocyte lineage (Olig2), myelin (MBP) and proliferation (Ki67) markers. Cell numbers were manually counted and $MBP^+$ area was calculated with an ImageJ plugin.

**(a-d)** Immunofluorescence analysis of **(a)** $MBP^+$ cell numbers, **(b)** percentage area, **(c)** total $Olig2^+$ cell numbers and **(d)** representative images of cultures analyzed (scale bar=100 µm), n=6 wells.
**(e,f)** Immunofluorescence analysis of **(e)** $Olig2^+Ki67^+$ cell numbers with **(f)** representative images (scale bar=100 µm), n=6 wells.
**(g,h)** Pure OPC were treated with 5% of Treg-conditioned media or control medium and were analyzed after 2 days for **(g)** $MBP^+$ cell numbers. **(h)** Representative image of OPC cultures analyzed (scale bar=50 µm), n=12 fields.
**(i,j)** Cultures of pure OPC seeded on DRG neurons were treated with 5% Treg-conditioned media or control medium and were analyzed after 4 days for differentiation ($CC1^+$) and myelination ($MBP^+$). DAPI staining identifies OPC nuclei. **(j)** Representative image of co-cultures in the presence or absence of Treg-conditioned medium, n=20 fields. Enlarged image scale bar = 50 µm.

Data shown are representative of at least 12 **(a,b,d)**, 3 **(c,g-j)** and 2 **(e,f)** independent experiments, mean +/- SEM, Student's t-test (cell counts) and Mann-Whitney tests (percentage area), $^{**}p<0.01$, $^{***}p<0.001$.

**Figure 4. CCN3 is produced by Treg and promotes oligodendrocyte differentiation and myelination.**

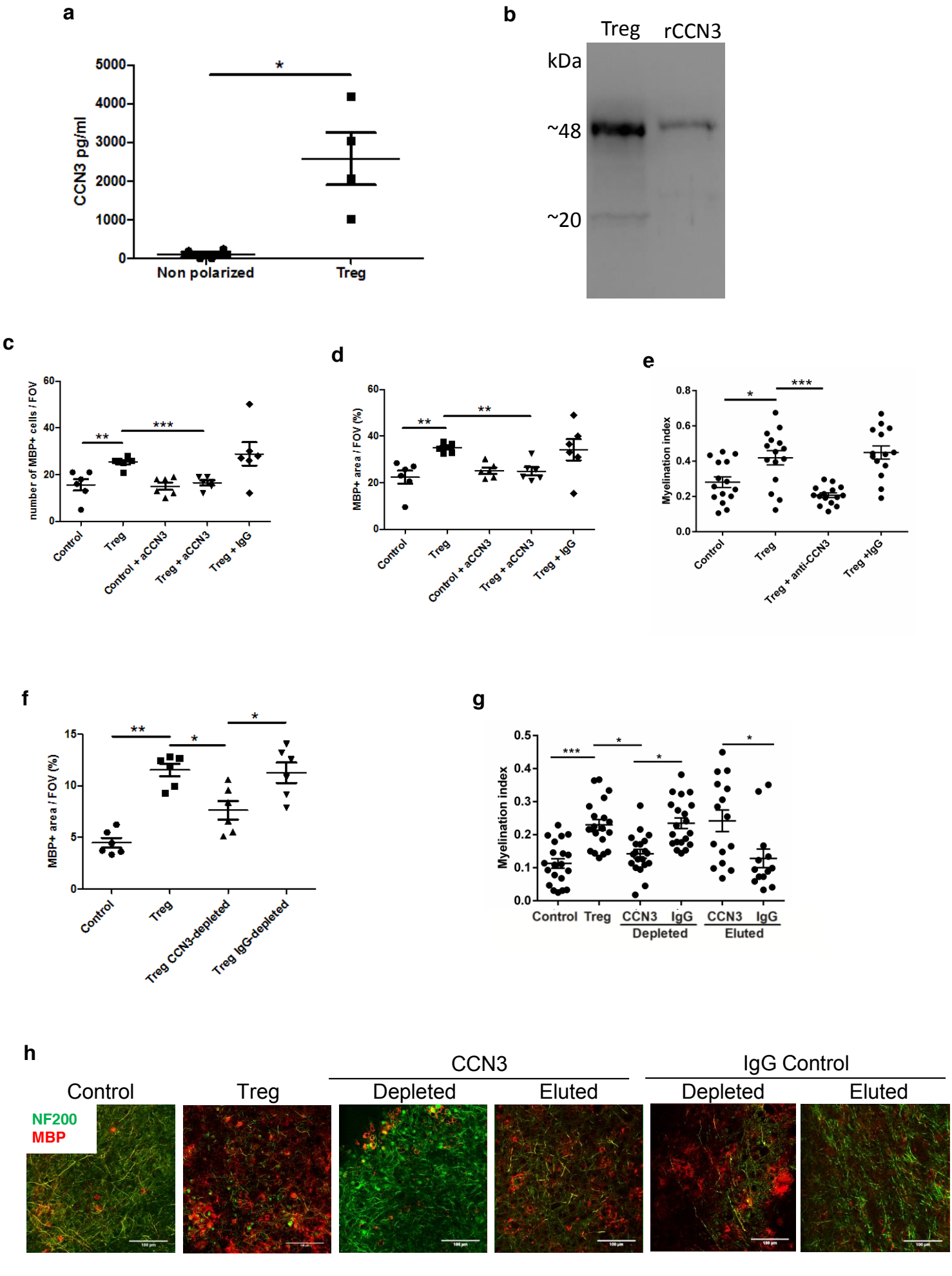

**Figure 4. CCN3 is produced by Treg and promotes oligodendrocyte differentiation and myelination**

**(a)** ELISA quantification of CCN3 in T cell conditioned media, n=4, Mann-Whitney test.
**(b)** Western blot analysis of CCN3 in Treg-conditioned medium. Recombinant CCN3 (rCCN3, 25 ng, R&D Systems) was used as a positive control. Samples were pre-enriched for CCN3 with heparin beads (GE Healthcare) overnight prior to western blotting.
**(c,d)** Mixed glial cells were treated with 5% Treg-conditioned medium, or medium control in the presence or absence of anti-CCN3 antibody and analyzed after 5 days for **(c)** $MBP^+$ cell numbers and **(d)** percentage area, n=6 wells, Student's t-test (counts) or Mann-Whitney tests (percentage area).
**(e)** Myelination index of brain stem slices treated with 5% Treg-conditioned media in the presence or absence of anti-CCN3 or isotype antibody for 7 days, n=15 fields of view from 3-6 slices/group, Student's t-test.
**(f)** Mixed glial cells were treated with 5% Treg-conditioned medium, or medium control with or without CCN3 depletion and analyzed after 5 days for $MBP^+$ percentage area, n=6 wells, Mann-Whitney test.
**(g,h)** Myelination index and representative images of brain slices treated for 7 days with 5% Treg-conditioned medium, or medium control with or without CCN3 depletion as well as eluted CCN3, n=3-5 fields of view from 3-4 slices/group, Mann-Whitney and Student's t tests (scale bar=100 μm).

Data shown are representative of at least 4 **(a)**, 2 **(b, f-h)** and 3 **(c-e)** independent experiments, mean +/- SEM, *p<0.05, **p<0.01, ***p<0.001.

**Supplementary Figure 1.**

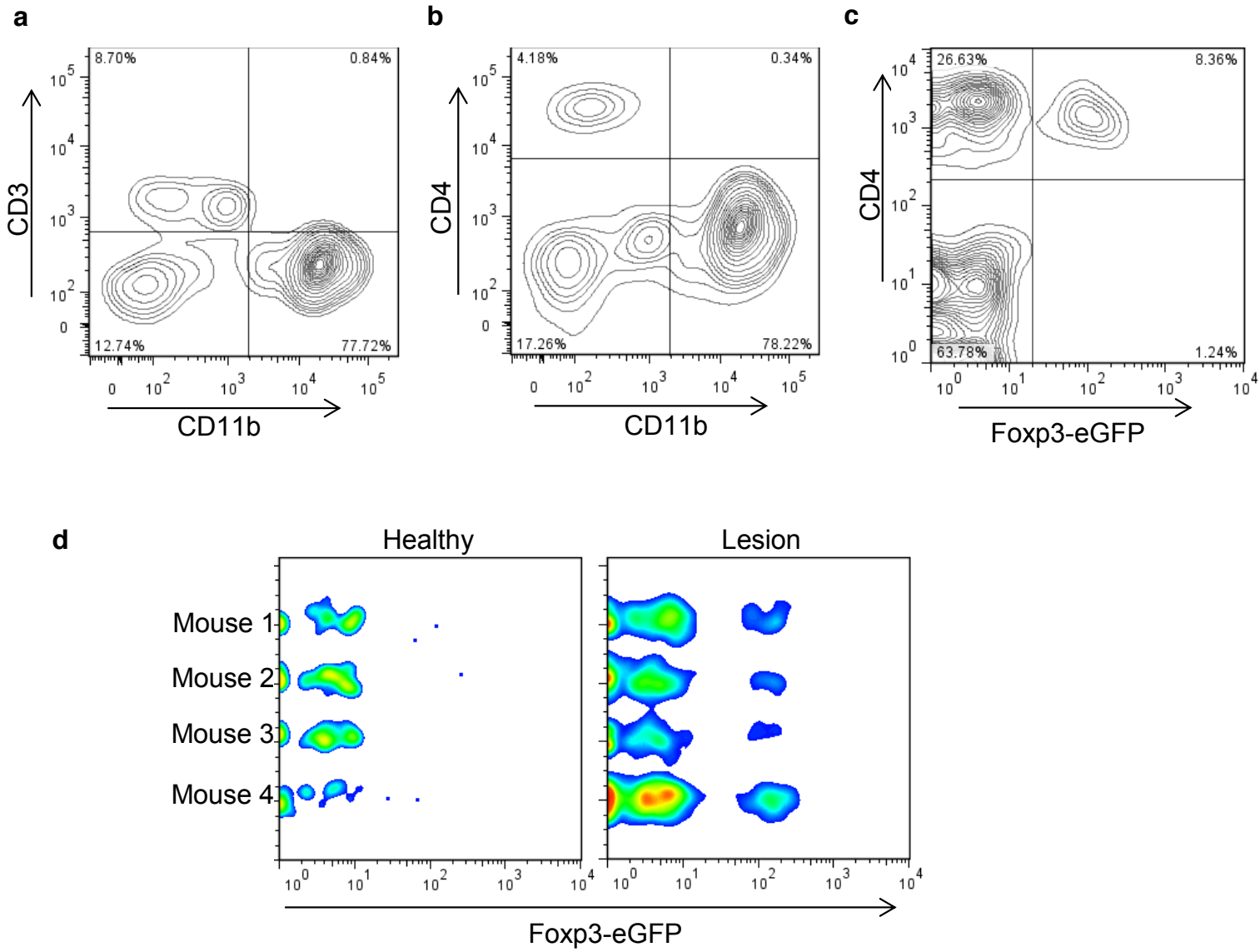

**Supplementary Figure 1. continued**

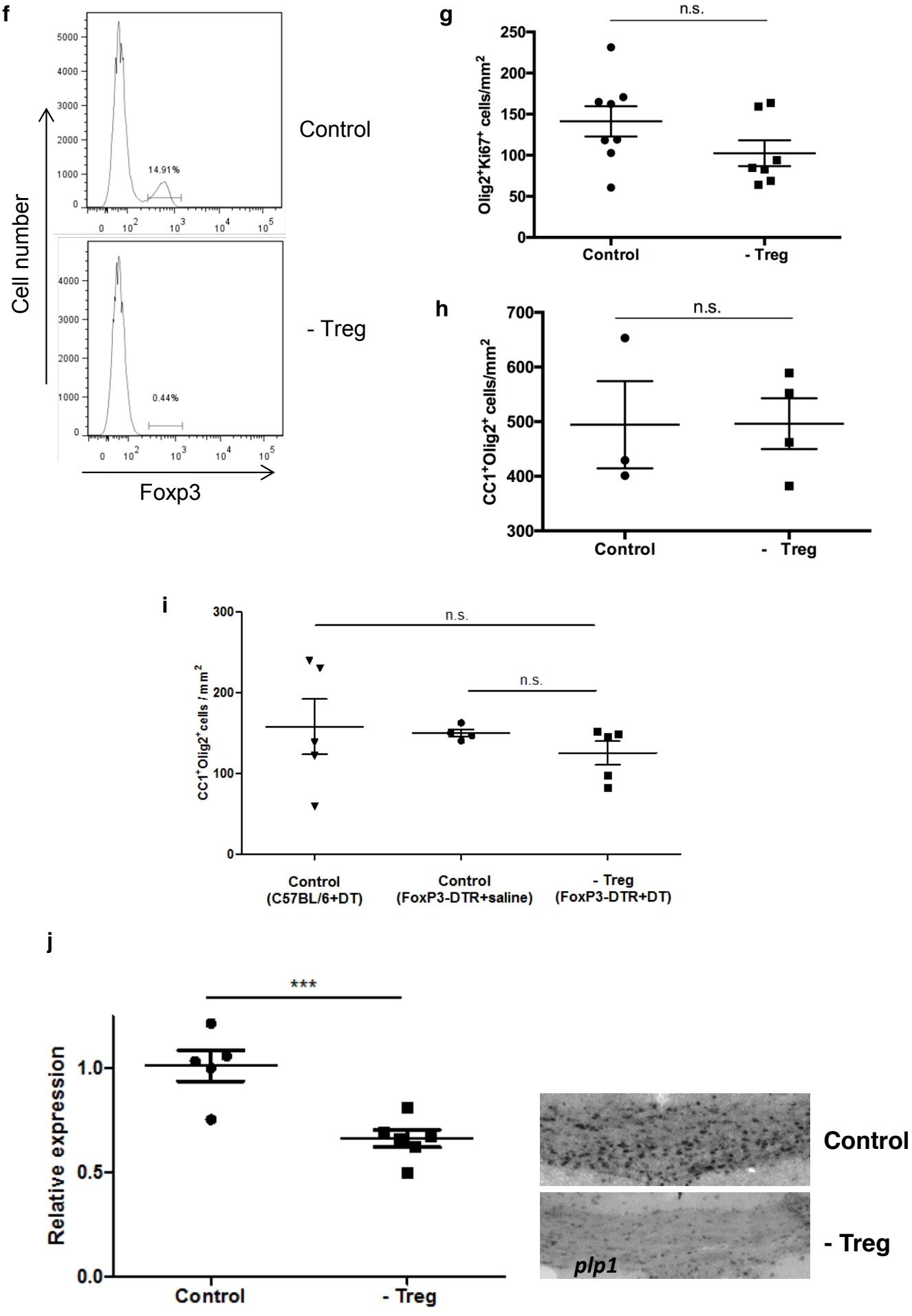

**Supplementary Figure 1. continued**

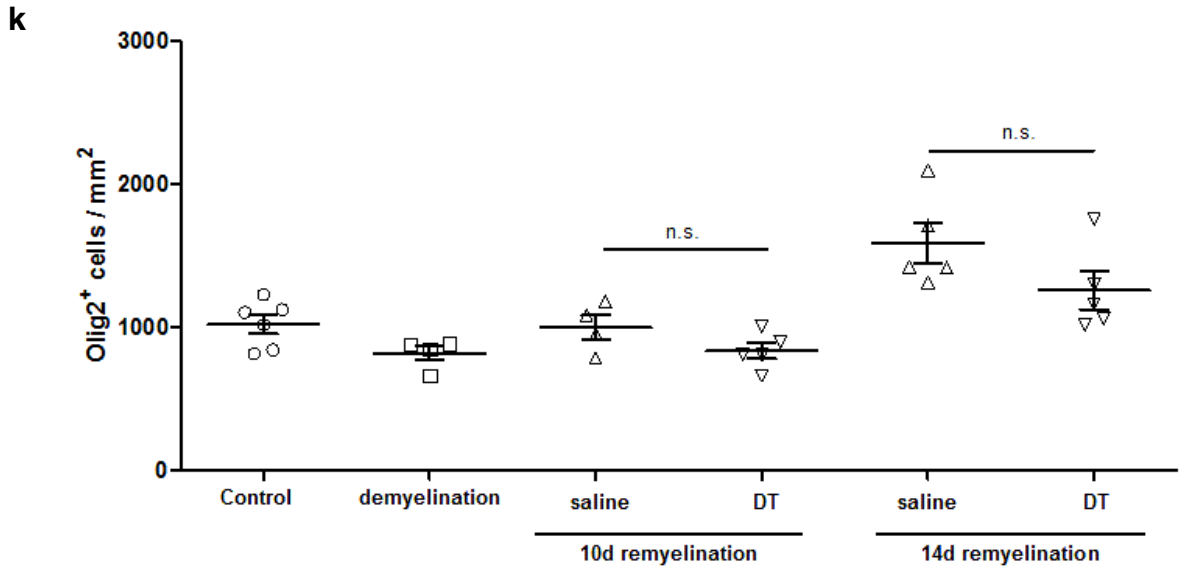


**Figure S1.** Fresh lesional spinal cord (lysolecithin) and brain (cuprizone) tissue of wildtype, Foxp3-DTR or Foxp3-eGFP mice was harvested and processed for flow cytometric analysis **(a-f),** immunofluorescence analysis **(g-i,k)** or mRNA analysis by qPCR and *in situ* hybridisation **(j).**

**(a-d)** Representative images of flow cytometric analysis of **(a)** $CD3^+$ T cells, **(b)** $CD4^+$ T cells and **(c,d)** $CD3^+CD4^+Foxp3^+$ Treg, in lesional spinal cord tissue gated on **(a,b)** $CD45^+$ cells, **(c)** $CD45^+CD3^+$ and (d) $CD45^+CD3^+CD4^+$ at 3 d.p.l.
**(e)** Quantitative immunophenotyping of T cell populations in healthy and lesioned spinal cord harvested at 3 d.p.l. and 11 d.p.l., gated on $CD45^+$ cells. n=4 mice per group.
**(f)** Representative flow cytometric analysis of $Foxp3^+$ Treg cells in fresh spleen from DT-treated C57BL/6 (control) and Foxp3-DTR mice (- Treg) at 14 d.p.l., gated on $CD4^+$ cells.
**(g)** $Olig2^+Ki67^+$ cells per lesion area of Foxp3-DTR mice at 10 d.p.l. with n=8 animals in control and n=7 animals in Treg-depleted group. Student's t test.
**(h)** $CC1^+Olig2^+$ cells per lesion area at 10 d.p.l. of mice with Treg depletion restricted to pre-lesioning phase, with n=3 animals in control and n=4 animals in Treg-depleted group.
**(i)** Immunohistochemical analysis of $CC1^+Olig2^+$ cells per lesion area of the corpus callosum at 10 days post-cuprizone withdrawal. n=5 animals for C57BL/6 DT-treated controls, n=4 animals for saline-treated Foxp3-DTR controls, n=5 animals for Treg-depleted Foxp3-DTR group; data represent analysis of 2-4 regions of corpus callosum per animal. Student's t-test used for control (C57BL/6) vs. –Treg
**(j)** *plp1* expression analysis in cerebellar tissue of control and Treg-depleted animals at 14 days post-cuprizone withdrawal by qPCR (left panel, normalized to *gapdh*) and by *in situ* hybridization in corpus callosum (right panel, representative images). n=5 animals (control) and n=6 animals in Treg-depleted group. Student's t test.
**(k)** Immunohistochemical analysis of total $Olig2^+$ cells per lesion area in the corpus callosum at 10 and 14 days post-cuprizone withdrawal. n=6 animals (control), n=4 animals (demyelination and 10 days control remyelination group), n=5 (all other remyelination groups); data represent analysis of 2-4 regions of corpus callosum per animal. Student's t test used for day 14.

Data shown are representative of at least 3 **(a-d, f),** 2 **(e, left panel)** or 1 **(e, right panel, g-k**) independent experiments. Mean +/- SEM, *$p<0.05$, ***$p<0.001$, Mann-Whitney test unless otherwise stated.

## Supplementary Figure 2.

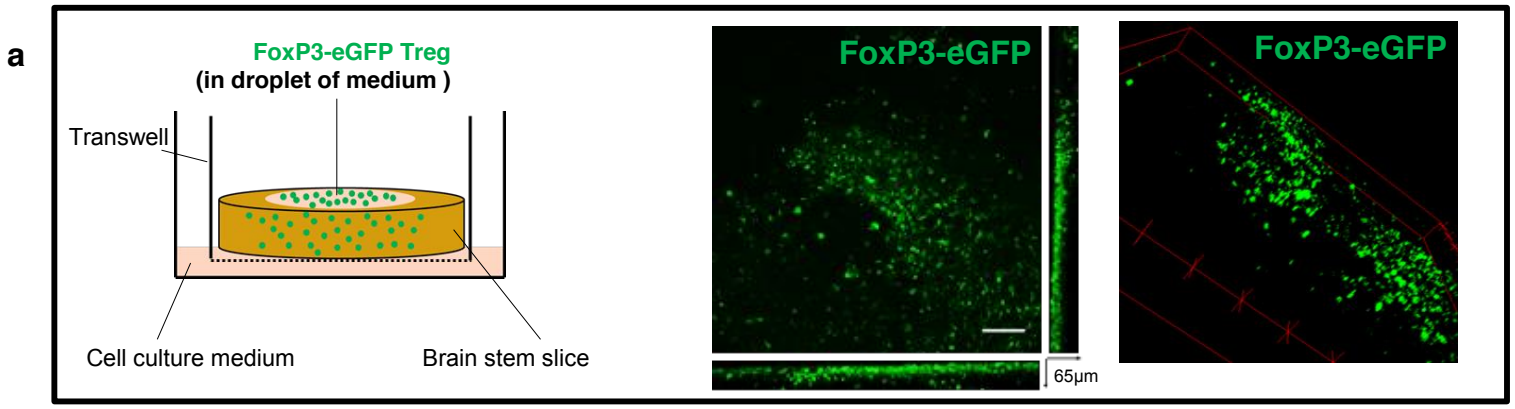


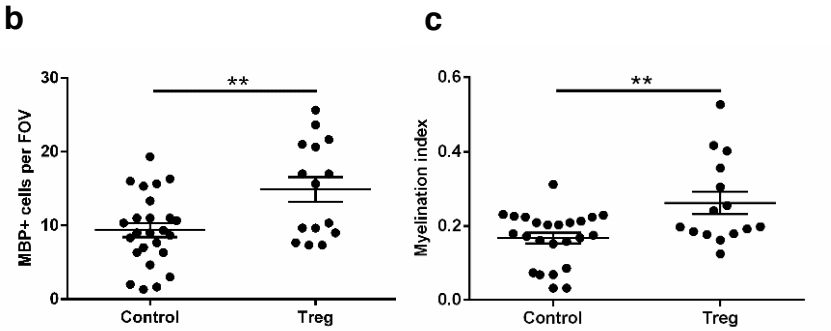


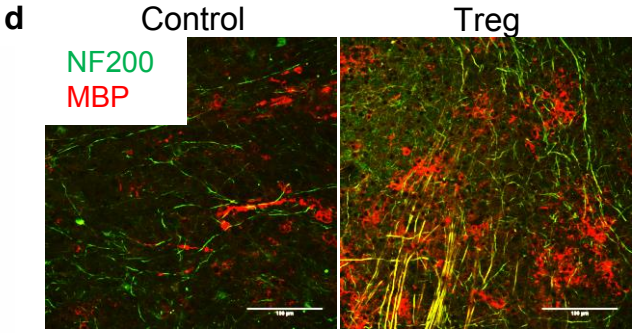


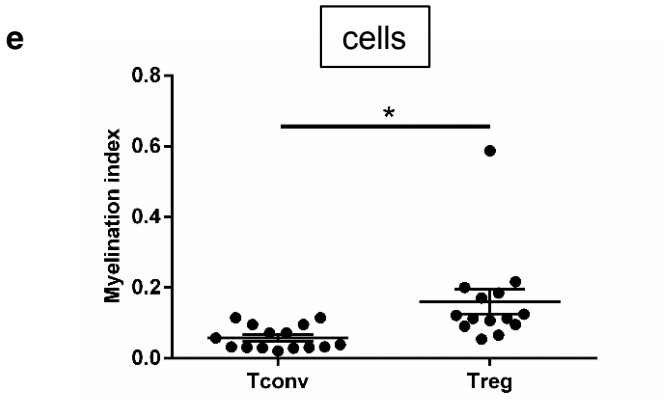


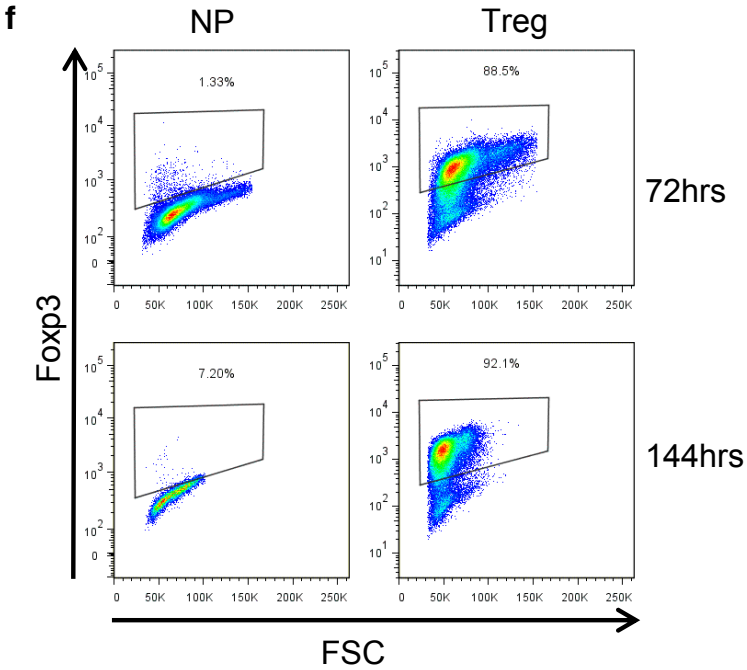


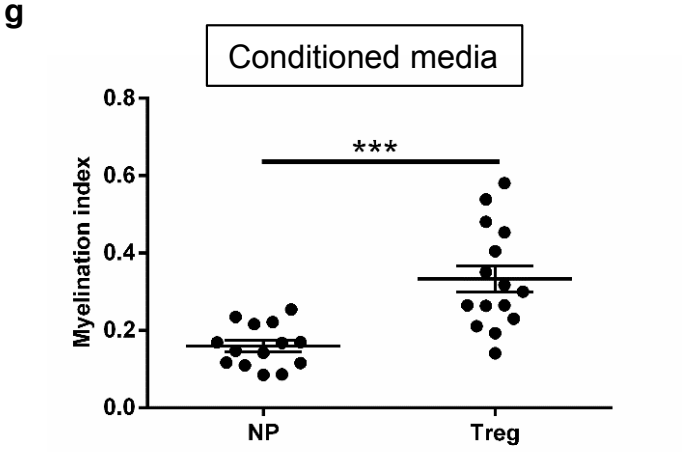

**Supplementary Figure 2.**

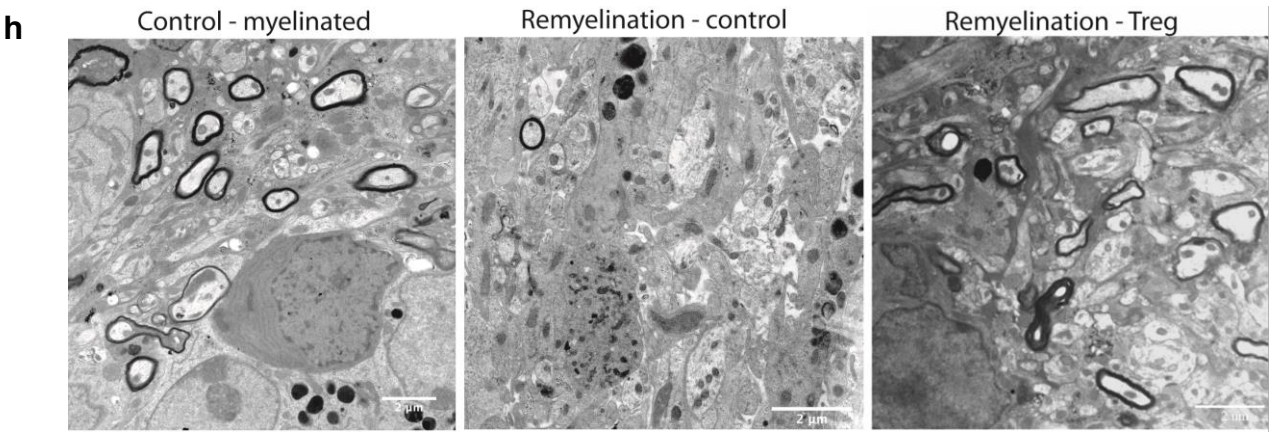


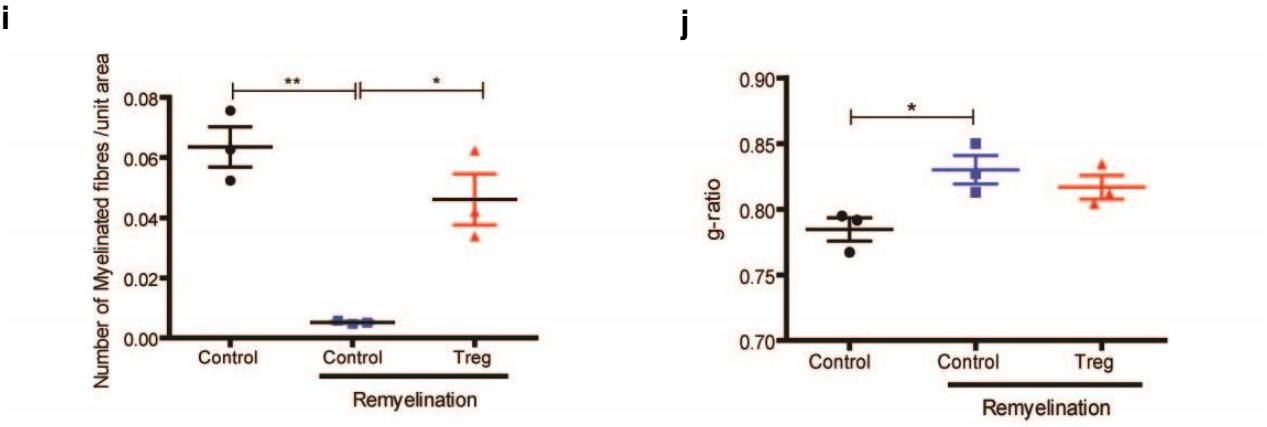


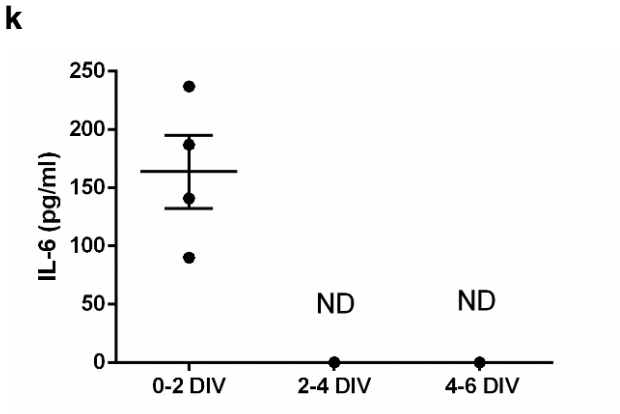

**Figure S2.** Brain stem slices from P0-P2 mouse pups were cultured in the presence or absence of FACS-purified T cells (**a-e**, 0-3 d.i.v.) or Treg-conditioned media (**g**, 0-7 d.i.v) or control medium (control). With the exception of (**a**), brain slices were fixed and stained for axonal (NF200) and myelin (MBP) markers. $MBP^+$ cells were manually counted and myelination index (myelin and axonal staining overlap, representing axonal ensheathment by myelin) was determined using an ImageJ plugin.

**(a)** Schematic diagram and 3D image of Foxp3-$eGFP^+$ Treg in organotypic brain slice cultures representing z-stack images at 3 d.i.v. (scale bar = 100 µm).
**(b,c)** Analysis of **(b)** $MBP^+$ cells per FOV and **(c)** myelination index, calculated with a customized ImageJ plugin as described in methods. Control n=24 FOV, Treg n=15 FOV from 3-6 slices/group, Student's t-test.
**(d)** Representative images of brain slices from **(b, c)** taken from a z-stack image (scale bar = 100 µm).
**(e)** Analysis of myelination index calculated with a custom ImageJ plugin. Tconv n=15 FOV and Treg n=14 FOV from 3-6 slices per group, Mann-Whitney test.
**(f)** Representative flow cytometric analysis of non-polarized (NP) T cells and Treg activated in RPMI medium for 72 hr followed by reactivation in brain slice medium for 72 hr. FSC = Forward Scatter.
**(g)** Analysis of myelination index calculated with a custom ImageJ plugin. NP n=14 FOV and Treg n=15 FOV from 3-6 slices per group, Student's t-test.
**(h-j)** Electron microscopic analysis of control (non-demyelinated) and remyelinating brain slices with and without Treg-conditioned medium. One-way ANOVA with Bonferroni post-test, n=3 slices/condition. *p<0.05, **p<0.01.
**(k)** ELISA of IL-6 in brain slice culture-conditioned media up to day 6 *in vitro*. n=4.

Data shown are representative of at least 2 **(a-e, g)** 7 **(f)** or 1 **(h-j)** independent experiments, mean +/- SEM, *p<0.05, **p<0.01, ***p<0.001.

**Supplementary Figure 3.**

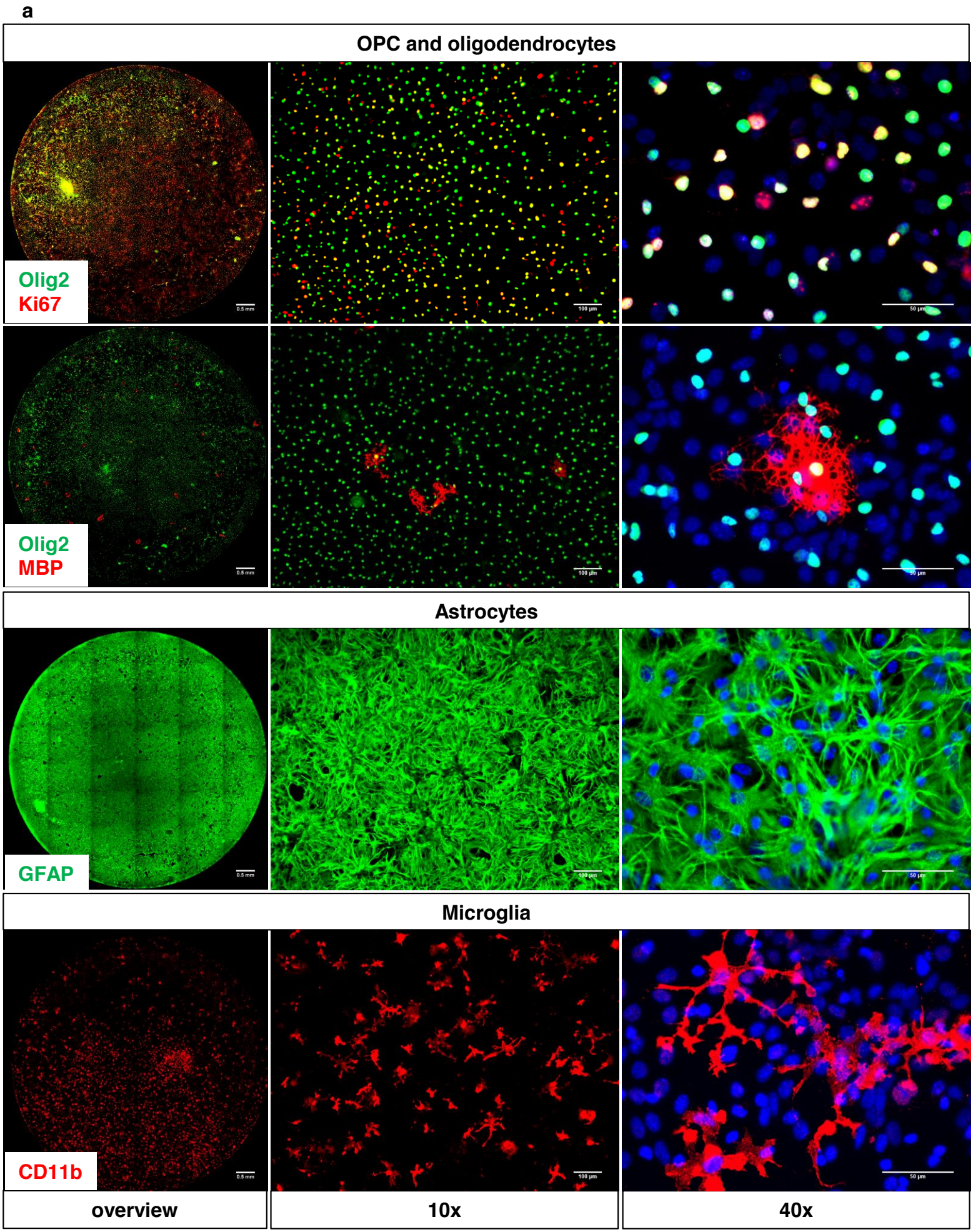

**Supplementary Figure 3. (continued)**

**b**

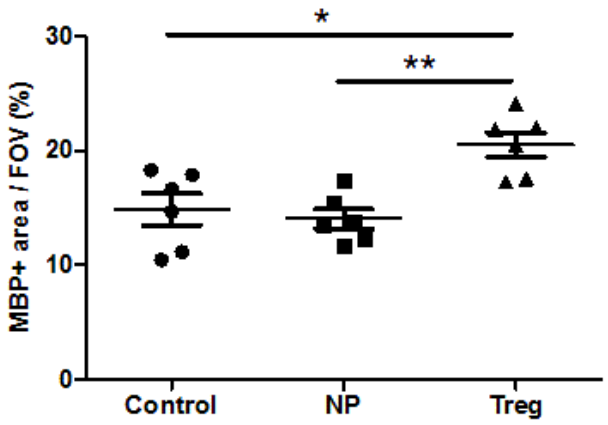


**c**

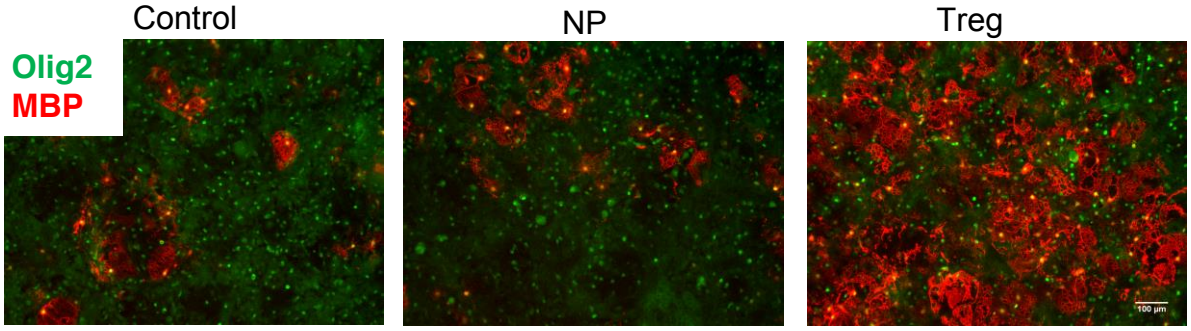


**d**

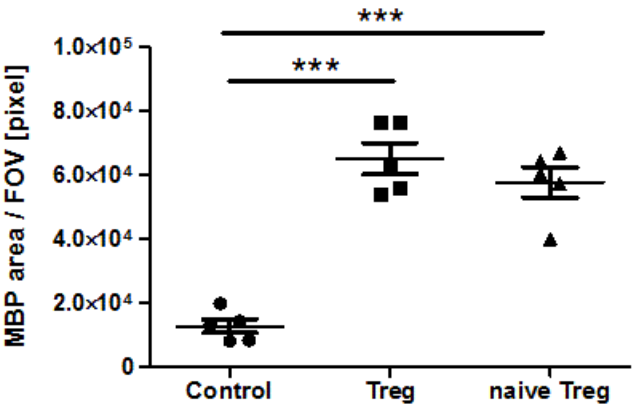


**e**

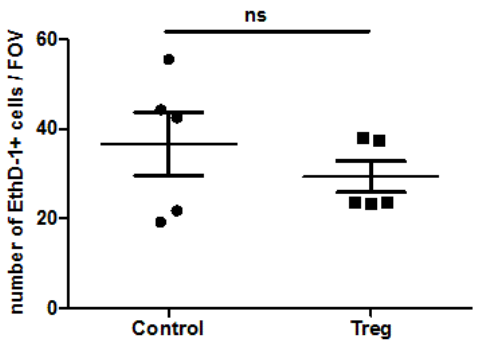


**f**

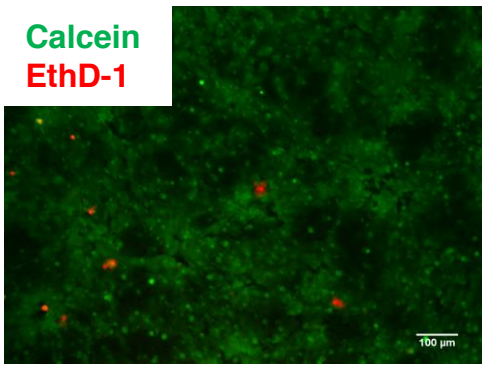

**Figure S3.** Mixed glial cultures were established from P2-7 C57BL/6 pups.

**(a)** Mixed glial cultures were stained for OPC (Olig2, Ki67), oligodendrocyte (Olig2, MBP), astrocyte (GFAP) and microglial (CD11b) markers after 1 week of culture. Nuclei were counterstained with DAPI (blue). Left panels depict a stitched image of the well of a 96-well plate (stitched images were taken at 10x) (scale bars from left to right panels = 500 µm, 100 µm, 50 µm).
**(b-f)** Mixed glial cells from P2-7 mouse pups were expanded for 7 days *in vitro* and then treated for 5 days with 5% Treg-conditioned medium, medium from non-polarized (NP) T cells or control medium (control) as indicated.
**(b, c)** Immunofluorescence analysis of $MBP^+$ percentage area and **(c)** representative images, n=6. (scale bar = 100 µm).
**(d)** Immunofluorescence analysis of $MBP^+$ area of cultures treated with Treg-conditioned media derived from total or naïve $CD4^+$ T cells, n=5.
**(e,f)** Immunofluorescence analysis of EthD-$1^+$ cell numbers and **(f)** representative images, n=5. (scale bar = 100 µm).

Data representative of **(b)** 3 and **(d,e)** 2 independent experiments, mean +/- SEM, unpaired student's t-test (counts) or Mann-Whitney test (percentage area), * $p<0.05$, ** $p<0.01$.

# Supplementary Figure 4.

**a**

| Location | Protein | NP | Treg | Treg |
|---|---|---|---|---|
| D3,4 | IL-10 | | | |
| E3,4 | Osteopontin | | | |
| C7,8 | GMCSF | | | |
| E9,10 | PDGF-AB | | | |
| C9,10 | HB-EGF | | | |
| D11,12 | MCP1/CCL2 | | | |
| D13, 14 | MIP1a/CCL3 | | | |
| A17,18 | CXCL16 | | | |
| D19,20 | MMP9 | | | |
| D21,22 | CCN3 | | | |

signal strength *
positive
not detectable

*compared to medium control

**b**

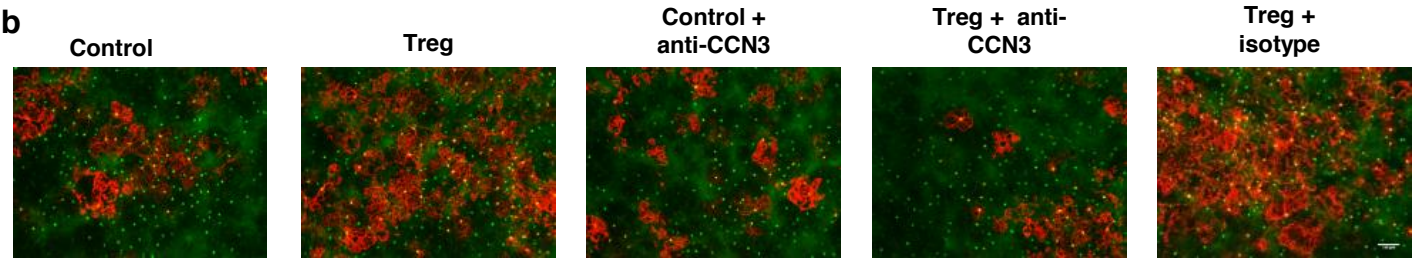


**c**

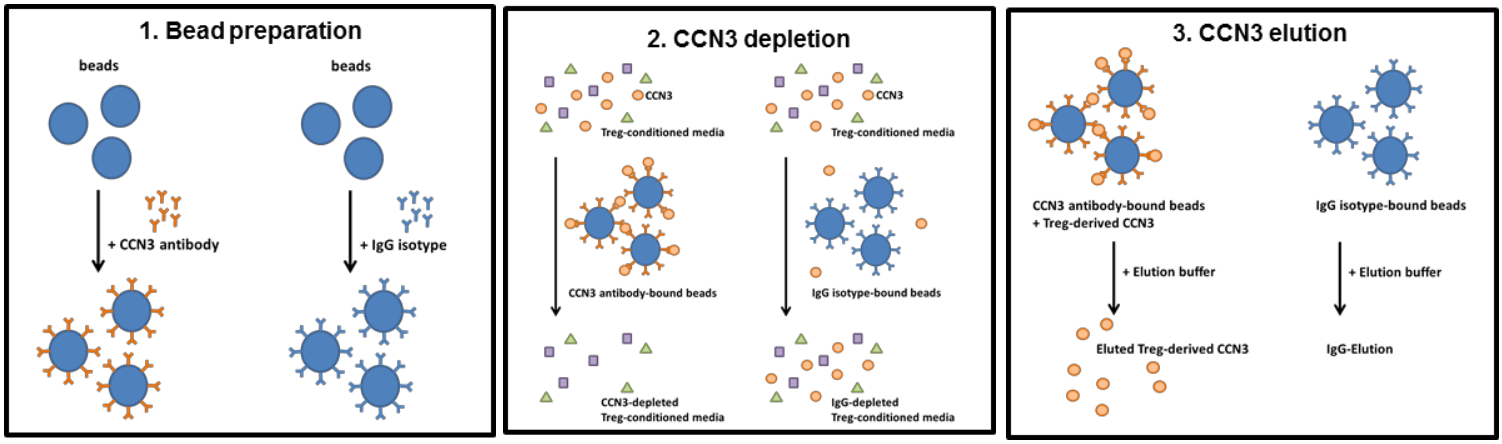


**d**

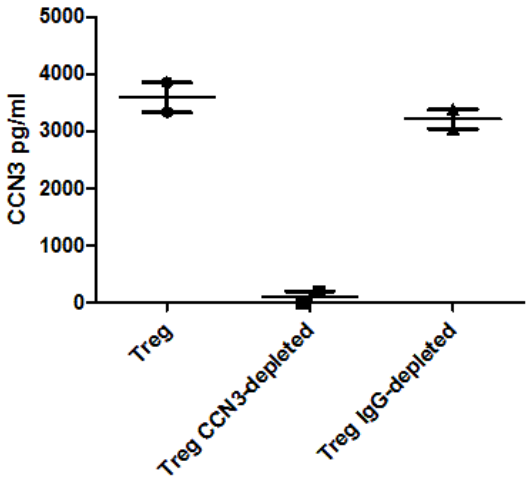

**Figure S4.**

**(a)** Semi-quantitative proteome profiler analysis of non-polarized (NP)- and Treg-conditioned media (2 independent batches) compared to cell culture medium only.
**(b)** Representative immunofluorescence images of mixed glial cultures stained for $Olig2^{+}MBP^{+}$ cells and analyzed quantitatively in Figure **4 c,d**. Green = Olig2, red = MBP, (scale bar = 100 µm).
**(c)** Schematic diagram of CCN3 depletion and elution from Treg-conditioned media.
**(d)** ELISA confirmation of CCN3 depletion from Treg-conditioned media.

Data representative of 1 **(a),** or at least 3 **(b,d)** biologically independent experiments.

**Supplementary movies**: Videos of z-stack imaging of representative remyelinating organotypic brain slices as described in Figure **2d-f**. Movie 1 = control, movie 2 = Treg, MBP stained red, NF200 stained green.